VISCOPLASTIC ANALYSIS OF A CONTINUOUS CYLINDRICAL OPENING SURROUNDED BY VOLCANIC TUFF

THESIS

AFIT/GAE/AA/82D-26 David E. Schmitz
Captain USAF

DEPARTMENT OF THE AIR FORCE
AIR UNIVERSITY (ATC)
AIR FORCE INSTITUTE OF TECHNOLOGY

Wright-Patterson Air Force Base, Ohio

DISCLAIMER NOTICE

THIS DOCUMENT IS BEST QUALITY PRACTICABLE. THE COPY FURNISHED TO DTIC CONTAINED A SIGNIFICANT NUMBER OF PAGES WHICH DO NOT REPRODUCE LEGIBLY.

VISCOPLASTIC ANALYSIS OF A CONTINUOUS CYLINDRICAL OPENING SURROUNDED BY VOLCANIC TUFF

THESIS

AFIT/GAE/AA/82D-26 David E. Schmitz
Captain USAF

VISCOPLASTIC ANALYSIS OF A CONTINUOUS CYLINDRICAL OPENING SURROUNDED BY VOLCANIC TUFF

THESIS

Presented to the Faculty of the School of Engineering
of the Air Force Institute of Technology
Air University
in Partial Fulfillment of the
Requirements for the Degree of
Master of Science

by
David E. Schmitz
Captain USAF
Graduate Aeronautical Engineering

December 1982

Acknowledgements

I would like to express my appreciation to Professor A. N. ("Dr. P") Palazotto for his guidance, advice, encouragement, and patience throughout the course of this study. I would also like to thank Captain Terry Hinnerichs and Captain Jim Smail, of the Air Force Weapons Laboratory, for their timely support of this project. Thanks also go to Dr. T. Nicholas and Captain Mike Bohun, of the Air Force Materials Laboratory, for arranging the needed computer resources.

I especially want to thank the two women in my life, Holly and Brandy. Their unyielding support in this endeavor was invaluable.

Contents

List of Figures

List of Tables

Abstract

The effect of a surface nuclear blast on a deep underground tunnel was studied using elastic-viscoplastic theory. Quasi-static and quasi-transient loadings were analyzed using a finite element model developed herein.

The computer program used is a two-dimensional plane stress/plane strain code using constant strain triangle elements. Constitutive equations proposed by Drucker and Prager were incorporated to account for the compressibility inherent to rock material. Plasticity was generated using the Drucker-Prager yield criteria incorporated in the Malvern flow law. Both viscoplastic and elasto-plastic material behavior were modeled using the viscoplastic theory.

The quasi-static analysis compared excellently to material behavior displayed in field studies and experimental work. Results obtained through the quasi-transient analysis give an appreciation of possible plastic zone growth. Additionally, a modification to the Drucker-Prager equations was proposed and found to show less plastic strain than the full equations. This is promising when considered in light of the fact that the Drucker-Prager equations have been known to allow too much plasticity at high pressure levels.

VISCOPLASTIC ANALYSIS OF A CONTINUOUS CYLINDRICAL OPENING SURROUNDED BY VOLCANIC TUFF

I. Introduction

Background

Until the mid 1970s, the United States based its intercontinental ballistic missiles (ICBMs) in shallow underground concrete silos. This system was considered sufficiently protective to allow the United States to survive a "first strike," thus, giving a "second strike" capability.

With the advent of higher yield warheads coupled with increasingly accurate delivery systems, the protection provided by the silo system became suspect, and the search for a new ICBM basing system began. One of the ideas which came out of the search is the Deep Missile Basing System, which envisions a network of tunnels dispersed throughout a land mass called a mesa. These tunnels are buried within the mesa, and are subjected to the natural in situ stresses, as well as the dynamic stresses resulting from the spherically propagating stress wave generated by a contact or near-surface blast (see Fig 1) (Ref 1).

The survivability of deep underground tunnels is a function of both the strength of the employed tunnel

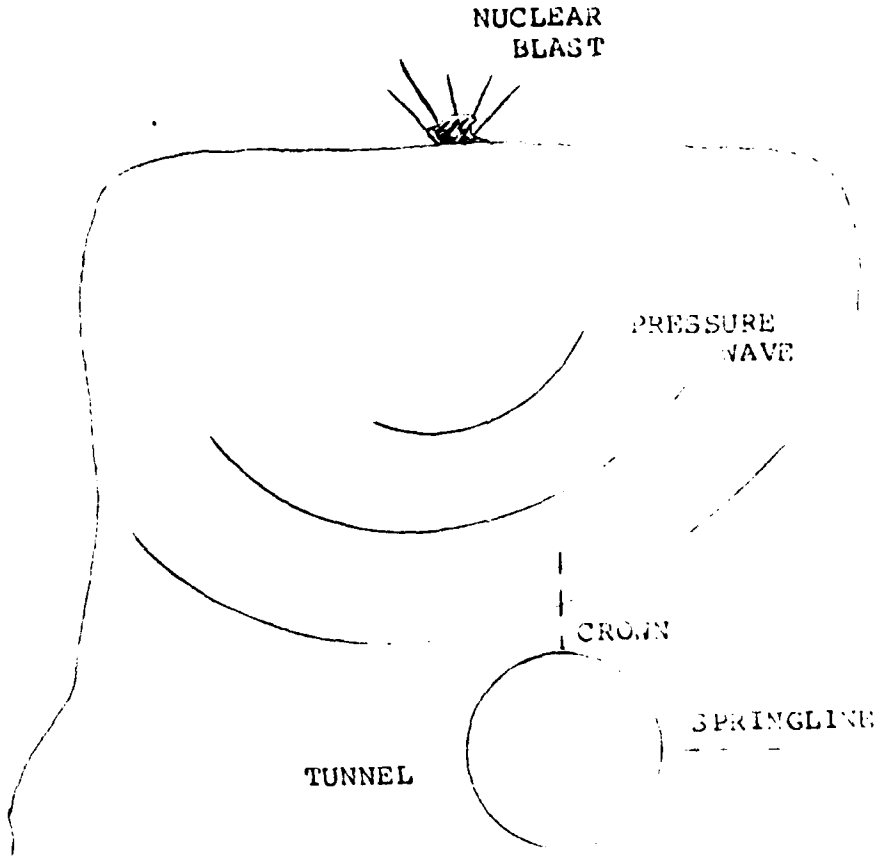

Fig 1. Cutaway of Deep Underground Missile Basing System

hardening measures (concrete liners, steel liners, rock bolts, etc.), and the strength of the surrounding rock. Economic tunnel design dictates minimum use of hardening techniques, taking advantage instead of the protective roc surrounding a tunnel (Ref 1). Therefore, the state of str ss in the tunnel/rock system must be estimated.

Approach

Experimental results reveal that loading near tunne levels from a surface nuclear blast causes failure in unli.ed tunnels, characterized by a distressed or loosened zone of rock at the springlines (the springline is perpendicular t the maximum load direction), and tension cracks at the cro.n. Since failure normally indicates plastic action, an elasti - plastic analysis is in order.

The Drucker-Prager plastic mate.i.l model represent one of the idealizations of real rock which entails appro.iate elastic constants, a yield function and a flow rule. Thre important characteristics of the real stress-strain curve are reflected in this model. First, elastic response is pronounced at lower loads. Second, as load is increased toward ultimate, the actual stress-strain curve has a.re.. bent over considerably so that the tangent modulus at th.s stage is a small fraction of the initial elastic modul.s. The perfectly plastic model represents a zero tangent mod.l.. Finally, the plastic behavior of rock is observed by havi. a residual strain when a complete unloading takes place bey.

the elastic range. This is in contrast to the nonlinear elastic idealization where unloading follows the initial path and the strain is fully recoverable. This last characteristic gives a distinction between a plastic and an elastic rock and, in the most fundamental sense, rock has been known to be a plastic rather than an elastic material (Ref 2).

The rock/tunnel system will be modeled using the finite element method, with an in-house code named VISCO. The rock will be treated for simplicity as a continuous and isotropic material. For the depths and yields of interest to deep missile basing systems, the pressure wave from a nuclear blast will probably have a significant rise time, on the order of 1 to 10 transit times, and be of fairly long duration, 100 to 200 transit times; in effect, making a quasi-static (steady state) approach appropriate. A quasi-transient analysis will also be done using appropriate rise times for each load level.

Objective

The objective of this thesis is to analyze the stress around the tunnel under the conditions of quasi-static and quasi-transient loading. This will be accomplished using viscoplastic theory incorporating the Drucker-Prager material model developed in Chapter II.

II. Theory

Plasticity

The behavior of materials beyond the elastic range is termed plastic, and can be characterized by an incomplete instantaneous recovery of strain upon removal of stress, a change in strain with time under constant load, a change in stress with time under constant deformation, a variation of mechanical properties with applied stress, or a variation of mechanical properties with temperature, direction, and position in the body. Thus, the implication is that the theory of elasticity can be used to make the first approximation of stresses, strains, and deformations in a structure under specified loading, and that various inelastic (plastic) theories can be used to estimate the deviation from elastic behavior that may occur and to estimate the total loads that a given structure can support before excessive deformation, fracture, or disintegration occurs (Ref 4).

Plasticity in Metals

Based on the above paragraph, total strain in a material can be written as

$$\varepsilon_{ij}^{\text{total}} = \varepsilon_{ij}^{\text{elastic}} + \varepsilon_{ij}^{\text{plastic}} \qquad (1)$$

The onset of plastic deformation (or yielding) is governed by a yield criterion, and post yield deformation occurs at a greatly reduced material stiffness. A yield criterion can be

written in the form $f(\sigma_{ij}) = k$, where f is some function and k is a material parameter to be determined experimentally. Experimental observations by Bridgman (Ref 3) indicate that plastic deformation of metals is essentially independent of hydrostatic pressure. Therefore, yield criteria can now be written as $f(J_2', J_3') = k$, where J_2' and J_3' are the second and third invariants of the deviatoric stresses

$$\sigma_{ij}' = \sigma_{ij} - \frac{1}{3}\delta_{ij}\sigma_{kk} \tag{2.2}$$

One of the simplest yield criterion is the Von Mises criterion $(J_2')^{\frac{1}{2}} = k$ shown in Fig 2, which depicts the yield surface and the locus of points upon which the principal normal stresses sum to zero (π plane). This may also be written as

$$\bar{\sigma} = \sqrt{3}(J_2')^{\frac{1}{2}} = \sqrt{3}k \tag{2.3}$$

where

$$J_2' = \frac{1}{2}\sigma_{ij}'\sigma_{ij}' \tag{2.4}$$

and $\bar{\sigma}$ is termed the effective stress, a stress invariant which measures the incremental change of the yield surface to an overstress. For the case of uniaxial tension ($\sigma_2 = 0$, $\sigma_3 = 0$) , $\sqrt{3}k$ is the uniaxial yield stress. For yielding to occur, $(J_2')^{\frac{1}{2}}$ must reach the value of $(J_2')^{\frac{1}{2}}$ in a uniaxial tension test. The Von Mises yield criterion implies that, if the state of stress lies on the yield surface, plastic flow occurs; if the state of stress is within the yield surface, elastic strains

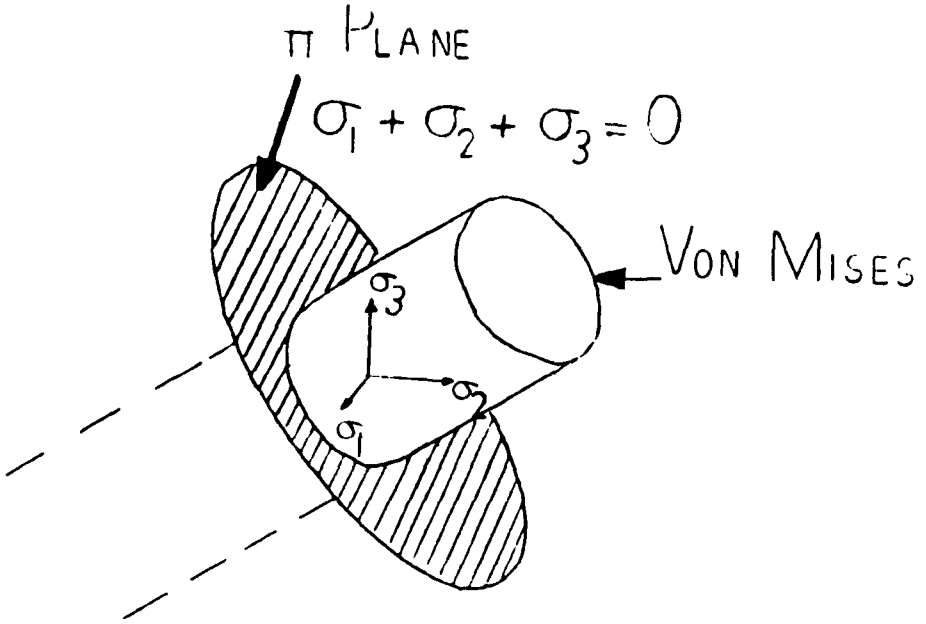

Fig 2. Geometrical Representation of the Von Mises Yield Surface in Principal Stress Space

occur. During plastic straining, this yield surface expands normal to itself (normality condition), thus, enforcing isotropic hardening within the plastic zone.

After the onset of plasticity, a so called equivalent yield stress function can be evaluated such that a gauge on plastic flow can be observed, and which increases as a function of the plastic strain. The equivalent yield stress can be written as

$$Y = \sigma_y + H' \varepsilon_p \qquad (2.5)$$

where σ_y is the uniaxial yield stress, H' is the slope of the strain-hardening portion of stress-strain curve, and ε_p is the plastic strain equivalent (Ref 5). Y is used as a universal stress-strain curve that governs the material's uniaxial inelastic behavior during loading, and is valid only when used with monotonically increasing loads. Once the onset of plasticity has occurred, increased plasticity will result only if $\bar{\sigma}$ exceeds Y .

Plasticity in Rock

Rock differs from metal in terms of plasticity because rock is a compressible material. While metals have one stress-strain curve, rocks have several which are a function of the confining stress $\sigma_1 - \sigma_3$. An increase in confining pressure significantly increases the compressive strength of rock. Most ductile materials have a fairly long plastic range before fracture occurs, where as brittle materials such as most

rocks have a very limited plastic range, if any, for uniaxial tension or compression. However, for triaxial loading, most brittle materials tend to show a plastic region where permanent deformation occurs. A yield criterion which accounts for hydrostatic stresses is the Drucker-Prager yield criterion (Ref 2), which modifies Von Mises by including J_1, the first stress invariant $(J_1 = \sigma_{11} + \sigma_{22} + \sigma_{33})$. Following the same analogy as with the Von Mises (including the normality condition), the Drucker-Prager criterion car be written as

$$\alpha J_1' + (J_2')^{\frac{1}{2}} = k' \qquad (2.6)$$

Therefore, plastic flow begins when the effective stress $\bar{\sigma} = \alpha J_1 + (J_2')^{\frac{1}{2}}$ exceeds k'; k' can be thought of as the yield stress, which in this case is a constant. The constant α describes the dilatation rate of soil, dilatant behavior being a volume increase under compression (Refs 6, 7, 17). Digressing somewhat, the Drucker-Prager yield criterion is an approximation to another criterion, the Mohr-Coulomb yield criterion. Note in Fig 3 that two Drucker-Prager yield surfaces are required to satisfy Mohr-Coulomb at the apices. Varying the radii is accomplished by using two equations for α and k'. For the outer apices (BDF)

$$\alpha = \frac{2 \sin\phi}{\sqrt{3}\ (3-\sin\phi)} \quad \text{and} \quad k' = \frac{6c\ (\cos\phi)}{\sqrt{3}\ (3-\sin\phi)} \qquad (2.7)$$

and for the inner apices (ACE)

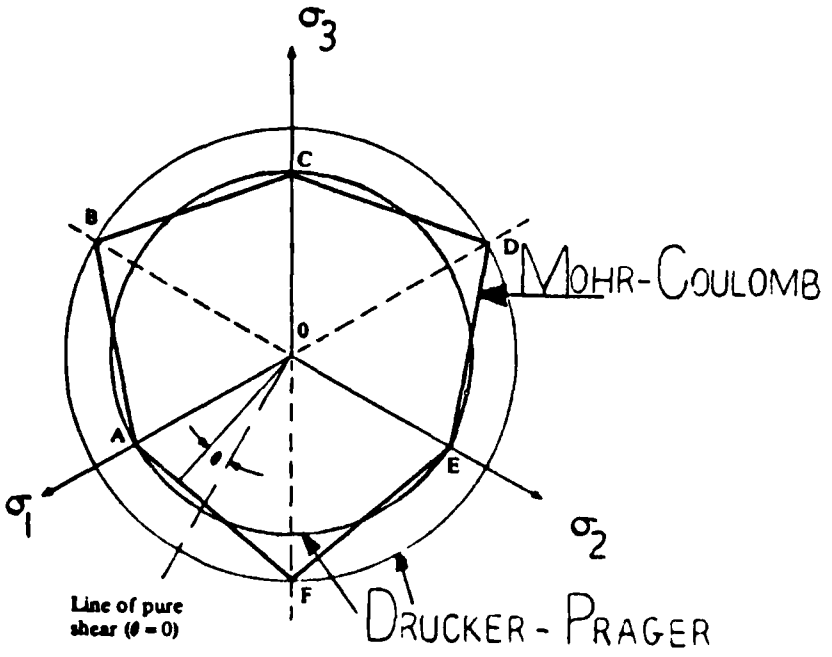

Fig 3. Two-Dimensional Representation of the Drucker-Prager and Mohr-Coulomb Yield Criteria

$$\alpha = \frac{2 \sin\phi}{\sqrt{3}\ (3 + \sin\phi)} \quad \text{and} \quad k' = \frac{6c\ (\cos\phi)}{\sqrt{3}\ (3 + \sin\phi)} \qquad (2.8)$$

C is the cohesion coefficient, a measure of the shear resistance between any two particles in a rock mass; shear resistance is the combined effect of cohesive resistance and frictional resistance. ϕ is the angle of internal friction, and is related to the fracture plane of a specimen occurring under a triaxial state of stress. Studies dealing with softer rocks and soils (Refs 10, 11) use Eq (2.8), while Eq (2.7) apply to stiffer materials such as harder rocks or concrete.

Viscoplasticity

A time-oriented viscoplastic finite element code called VISCO is used in this study. Time rate effects are always present to some degree in all inelastic deformations. Whether or not their inclusion has a significant influence on the prediction of the material behavior depends upon several factors. In the study of structural components under static loading at normal temperatures, it is accepted that time rate effects are generally not important and the conventional theory of plasticity, as described above, models the behavior adequately. However, some materials, especially at high temperatures, exhibit simultaneously the phenomena of creep and viscoplasticity. Creep can be defined as a redistribution of stress and/or strain with time under elastic material response while viscoplasticity is a time dependent plastic

deformation (Ref 5). A viscoplastic analysis increments time under full loading, while an elastic plastic analysis increments only the load.

The concept of viscoplastic material behavior is detailed through the use of the one-dimensional rheological model in Fig 4. The friction slider develops a stress σ_p, becoming active only if $\sigma > Y$, where Y is as above. The excess stress $\sigma_d = \sigma - \sigma_p$ is carried by the viscous dashpot. Instantaneous elastic response is carried via the spring. This model, specifically the dashpot, allows the stress level to instantaneously exceed the value prescribed by plasticity theory, the solution tending to a steady state condition with time (Ref 5).

Viscoplastic strain in rate form can be written as

$$\dot{\varepsilon}^{vp}_{ij} = \gamma < \Phi(F) > \frac{\partial F}{\partial \sigma} \qquad (2.9)$$

where

$$<\Phi(F)> = \Phi(F) \quad \text{for} \quad F > 0 \qquad (2.10)$$

$$<\Phi(F)> = 0 \quad \text{for} \quad F \leq 0 \qquad (2.11)$$

γ is a fluidity parameter controlling plastic flow rate, and is normally derived from uniaxial yield tests. $\frac{\partial F}{\partial \sigma}$ is the flow vector a for the associated plasticity which governs strain in the plastic region. The form of $\Phi(F)$ used in VISCO is

$$\Phi(F) = \left(\frac{F - F_o}{F_o} \right) \qquad (2.12)$$

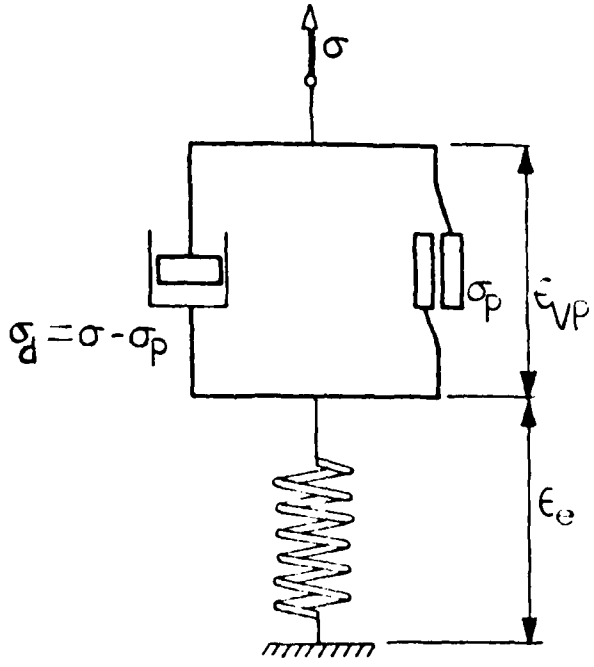

Fig 4. One-Dimensional Elastic-Viscoplastic Model

where F corresponds to $\bar{\sigma}$ (effective stress) and F_o corresponds to Y (equivalent yield stress) as described previously. Using the Von Mises flow vector (Ref 5) results in the VISCO definition of the viscoplastic strain rate

$$\dot{\varepsilon}^{vp}_{ij} = \gamma \left[\frac{\bar{\sigma}}{Y} - 1 \right] \frac{\sqrt{3}\, \sigma'_{ij}}{2\sqrt{J'_2}} \tag{2.13}$$

where σ'_{ij} are the deviatoric stresses.

Using the Drucker-Prager flow vector and recalling that $Y = k'$ and $\bar{\sigma} = \alpha J_1 + (J'_2)^{\frac{1}{2}}$ the viscoplastic strain rate can be written as (Ref 6)

$$\dot{\varepsilon}^{vp}_{ij} = \gamma \left[\frac{\bar{\sigma}}{k'} - 1 \right] \left[a_{ij} \right] \tag{2.14}$$

where

$$a_{ij} = \alpha + \frac{\sigma'_{ij}}{2(J'_2)^{\frac{1}{2}}} \quad \text{when} \quad i = j \tag{2.15}$$

$$a_{ij} = \frac{\sigma'_{ij}}{(J'_2)^{\frac{1}{2}}} \quad \text{when} \quad i \neq j \tag{2.16}$$

The generated plastic strain rates are multiplied by a time increment to yield plastic strains. As noted earlier, a steady state analysis will also be done. Under this condition, the key to using VISCO is the fluidity parameter γ. Perzyna showed that the constitutive equations of plastic flow theory result as a limiting case from the more general

constitutive equations of the viscoplastic theory as γ approaches infinity (Ref 6). The definition of steady state considering a finite γ in conjunction with Eq (2.14) will be discussed later.

III. VISCO Computer Program

VISCO is a plane strain/plane stress finite element code utilizing constant strain triangle elements. Because the program was initially designed for crack growth analysis, it uses a Gauss-Seidel iterative solution technique employing the initial stress method (Ref 10) to solve the equilibrium equation

$$[k]\{d\} = \{R\} \tag{3.1}$$

where $[k]$ is normally highly banded and stored in compacted form (retaining only non-zero terms), and $\{d\}$ is the nodal displacement vector.

As indicated above, once an element yields, the equivalent yield stress increases as a function of the plastic strain. This can be thought of as nonlinearity induced through material property changes. Two procedures exist to account for the effects of plasticity: one procedure reformulates the matrix each time an element experiences plastic deformation and is, therefore, both time consuming and expensive. The second procedure is called the residual force method in which the elastic stiffness matrix is used throughout the analysis and the effects of plasticity are treated as an applied load to be added to $\{R\}$.

If the elasto-plastic stiffness matrix is written as

$$[k]^P = [k]^E - [k]^C \tag{3.2}$$

where $[k]^C$ is the correction to the elastic stiffness matrix at a given stage in the analysis. Equation (3.1) for a particular load increment i becomes

$$([k]^E - [k_i]^C)\{\Delta d_i\} = \{\Delta R_i\} \tag{3.3}$$

and

$$[k]^E \{\Delta d_i\} = \{\Delta R_i\} + [k_i]^C \{\Delta d_i\} \tag{3.4}$$

Defining

$$\{\Delta d_i\} = \{\Delta d_i\}^E + \{\Delta d_i\}^P \tag{3.5}$$

where $\{\Delta d_i\}$ is the incremental displacement

then

$$[k]^E (\{\Delta d_i\}^E + \{\Delta d_i\}^P) = \{\Delta R_i\} + [k_i]^C (\{\Delta d_i\}^E + \{\Delta d_i\}^P) \tag{3.6}$$

from the elastic analysis

$$[k]^E \{\Delta d_i\}^E = \{\Delta R_i\} \tag{3.7}$$

so that

$$[k]^E \{\Delta d_i\}^P = [k_i]^C (\{\Delta d_i\}^E + \{\Delta d_i\}^P) = \Delta P \tag{3.8}$$

In short, the additional displacements due to plasticity can be solved by applying a corrective force ΔP to the elastic system (Ref 11).

The residual force method can be utilized even for a viscoplastic solution by incorporating a time step algorithm as follows (Ref 9):

1. Increment time so that $t = t^{i-1} + dt^i$

2. Compute the plastic strain increment as described in above Eqs (2.14), (2.15), $\{d\epsilon^P_{ij}\}^i = \{\dot{\epsilon}^P_{ij}\}^i \, dt^i$ and add to the preceding plastic strain.

3. Compute the plastic load vector

$$\{P\}^{i-1} = \int_{vol} [B]\ [k]\ \{\epsilon^P_{ij}\}^i \, dvol$$

where $[B]$ is the constant strain triangle strain-displacement matrix.

4. Compute the external load vector

$$\{R\}^i = \{R\}^{i-1} + \{\dot{R}\}dt^i$$

5. Compute nodal displacements

$$\{d\}^i = [k]^{-1} \left(\{R\}^i + \{P\}^{i-1}\right)$$

6. Compute current total strain

$$\{\epsilon_{ij}\}^i = [B]\ \{d\}^i$$

7. Compute current stress

$$\{\sigma_{ij}\}^i = [k]\ \left(\{\epsilon_{ij}\}^i - \{\epsilon^P_{ij}\}^i\right)$$

8. Insure the viscoplastic strain rate $\{\dot{\varepsilon}^{P}_{ij}\}^{i}$ in each element has reached tolerance limits and, if so, then repeat steps 1-8 until desired simulation time is reached.

IV. Rock Mechanics

The state of stress at a point strongly influences the strength, stiffness, ductility and creep properties of rock. Figure 5 shows variation in confining pressure, $\sigma_1 - \sigma_3$ versus axial strain for Sandston (Ref 13). Here, as in the remainder of this report (unless otherwise noted), all displayed stresses are compressive. The increase in confining pressure results in a significant increase in ultimate strength as well as a larger strain at failure. Also, plastic strains before ultimate failure (fracture) increase with confining pressure. The Drucker-Prager yield criterion accounts for confining pressure by including the first stress invariant (J_1 in Eq (2.6)), and also through the two material parameters C and ϕ defined above. C and ϕ are normally derived from triaxial test data using Mohr's circles as shown in Fig 6. Note that σ_i values are stresses at failure; in essence, the circles represent the material failure surface as a function of confining pressure. An alternative method was used here, in which C was derived from a known ϕ value and uniaxial test data. Using the spherical stress component $I = \frac{\sigma_x + \sigma_y + \sigma_z}{3}$ and recalling that $\sigma_{xy} = \frac{\sigma_x - \sigma_z}{2}$ then for a uniaxial test $I = \frac{\sigma_x}{3}$ and $\sigma_{xy} = \frac{\sigma_x}{2}$ which yields a point on a plot of σ_{xy} versus I (not shown). Using a sponsor supplied (from an unpublished report) slope of $\phi = 18^\circ$, a σ_{xy} intercept is determined and is used as the value for

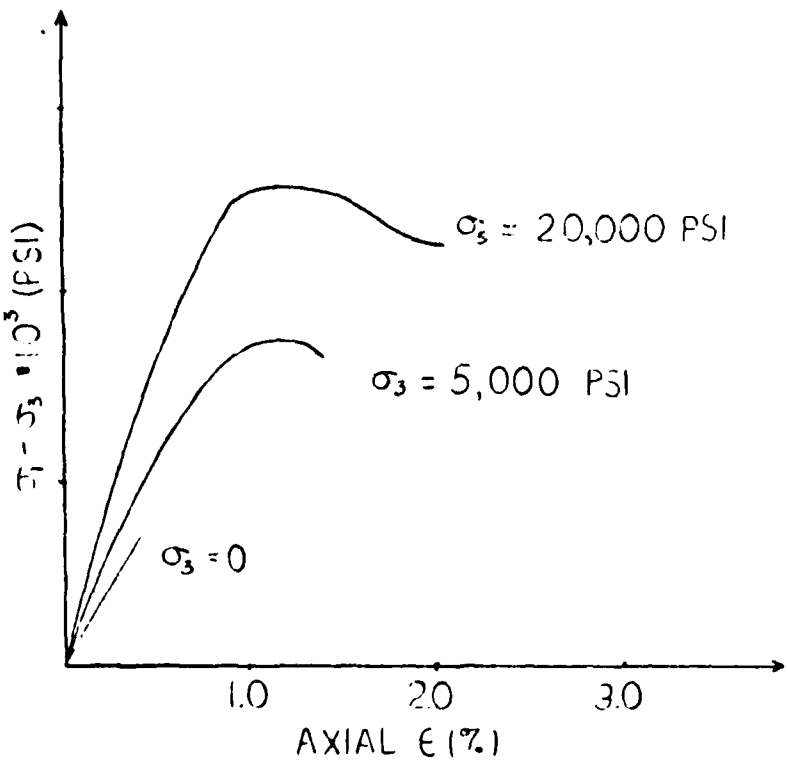

Fig 5. Variation of Stress-Strain and Strength Properties of Berea Sandstone

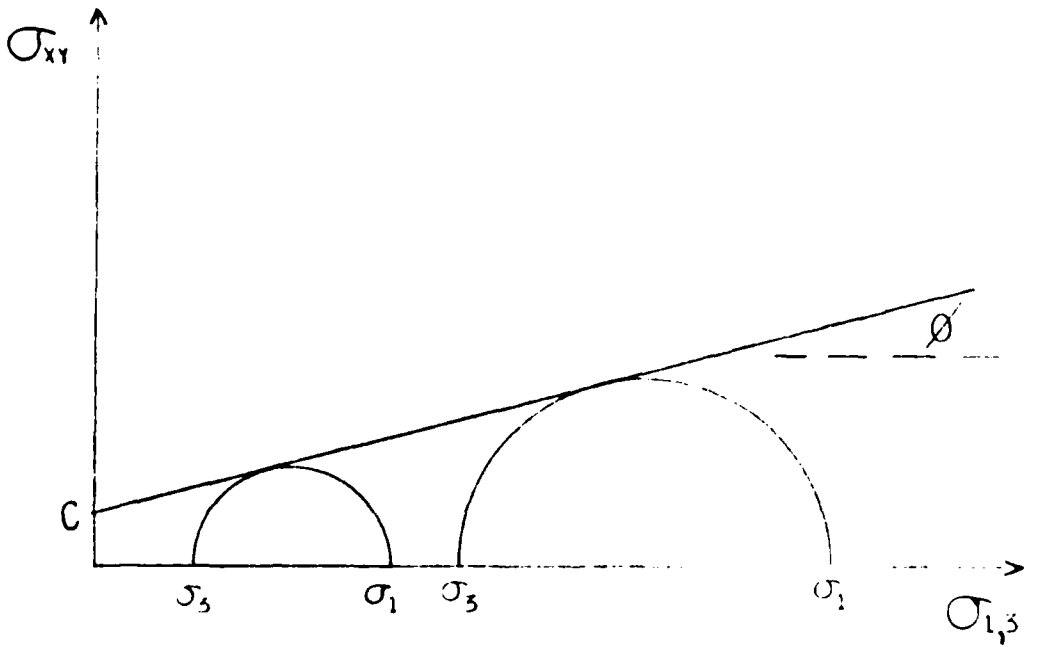

Fig 6. Deriving Material Parameters from Mohr's Circle Plots at Failure

C (in equation form $C = \sigma_x(\frac{1}{2} - \frac{1}{3}\tan 18°)$) . Using this method with given (Ref 7) triaxial data generated C values within 10% of known values. All material values for Tuff as used in this effort are presented in Table 1 (E, ϕ, and ν were supplied by the sponsor; all others are derived).

TABLE 1

Tuff Material Parameters

Parameter	Value
E	1.15E6 psi
ϕ	18°
C	980.7 psi
k'	976.4 psi
α	.1078
ν	.33

V. Modeling

Mesh Size

Since the size of the modeled section for this study had the potential to become very large, it was necessary to discover early a satisfactory mesh size limit. Mesh grading was also considered in conjunction with appropriate aspect ratios, where aspect ratio (AR) is the ratio of triangle height to width (not greater than AR=3) (Ref 14).

Timoshenko (Ref 15) gives a closed form elastic solution to the problem of a hole in a plate under uniaxial tension or compression, based on a ratio of d to a , where d is the plate half-width and a is the radius of the hole (Fig 7). Values of the stress concentration factor k_c at the crown and springline were used as the basis for determining the fineness of the mesh around the cutout. The radius of the hole is problem dependent; thus, determining d for any given d/a ratio. Arbitrarily selecting a d/a ratio of 5, with a given as 60 inches, yields a d value of 300 inches for the half-plate width. Using an element size of 6 inches by 12 inches (AR=2) near the hole yielded values of 2.97 for σ_y at the springline, and -1.01 for σ_x at the crown. Comparing to Timoshenko's values of 3.08 for σ_y and -1.0 for σ_x , gave acceptable errors of 3.56% and 1.0% respectively.

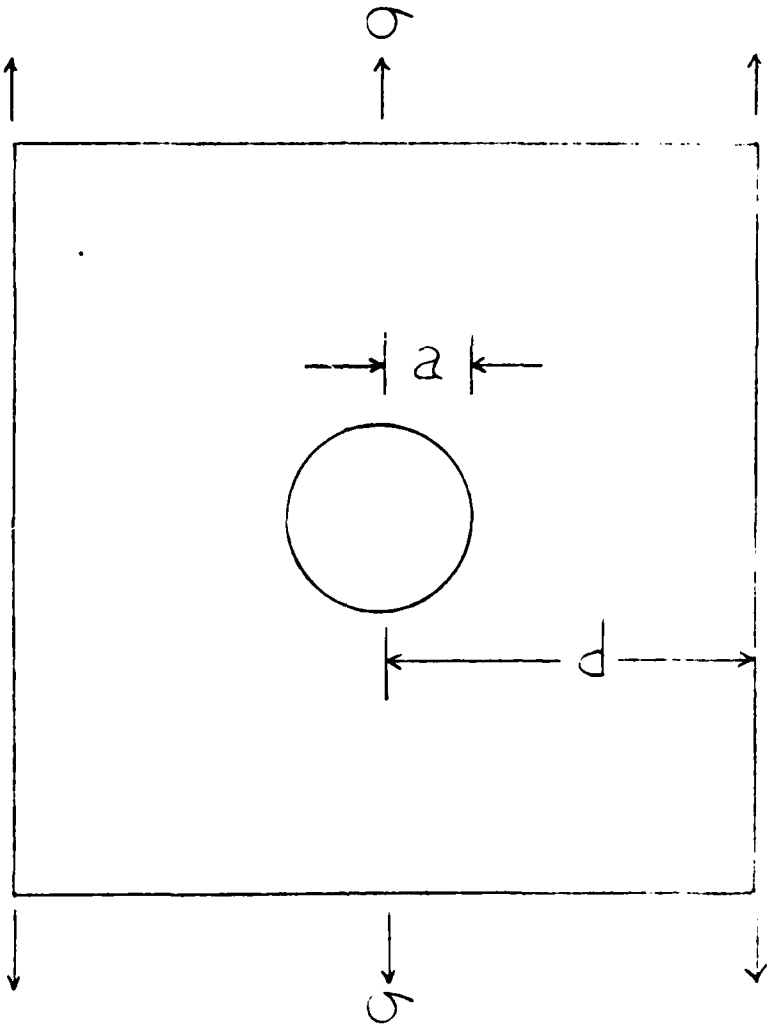

Fig 7. Plate Under Uniaxial Loading

Model Size

The in situ state of stress in a geological mass is the natural state of stress at any given point. Baker, et al (Ref 11) used a finite element model employing both elastic and elasto-plastic theory to analyze a deep tunnel in a rock mass. Setting both horizontal and vertical boundaries at 10 radii (600 inches) gave elastic in situ stresses in agreement with Baker's (maximum errors of 4.0% for σ_y and 6% for σ_x on a horizontal axis through the tunnel, see Fig 8). Summarizing, the model is 600 inches square with 323 nodes and 576 elements. The smallest elements are next to the cutout and are 6 inches by 12 inches. As Fig 9 shows, boundaries not loaded are fixed to move in only one direction.

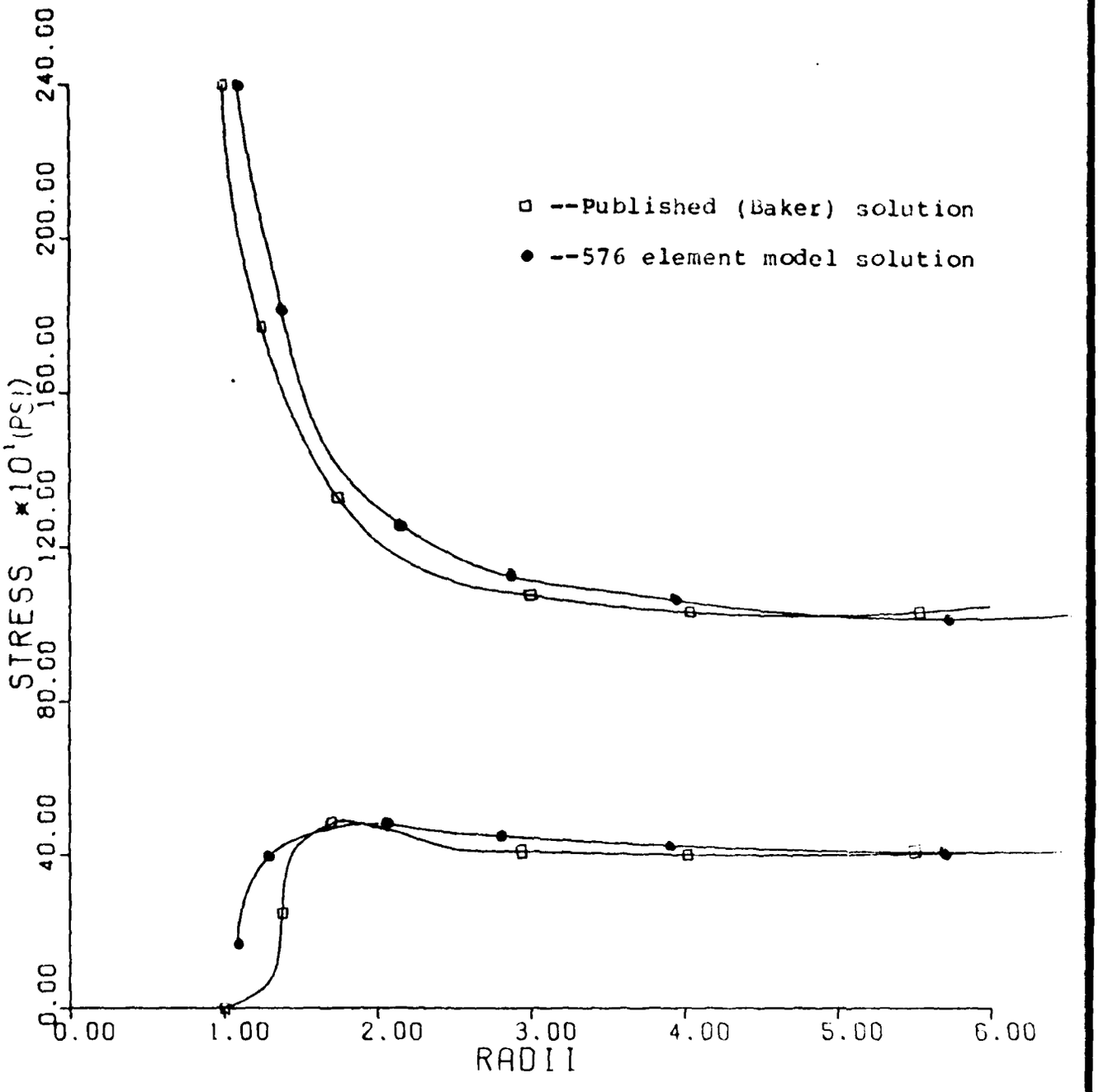

Fig 8. σ_x and σ_y Comparison Between Published Results (Ref 11) and 576 Element Model

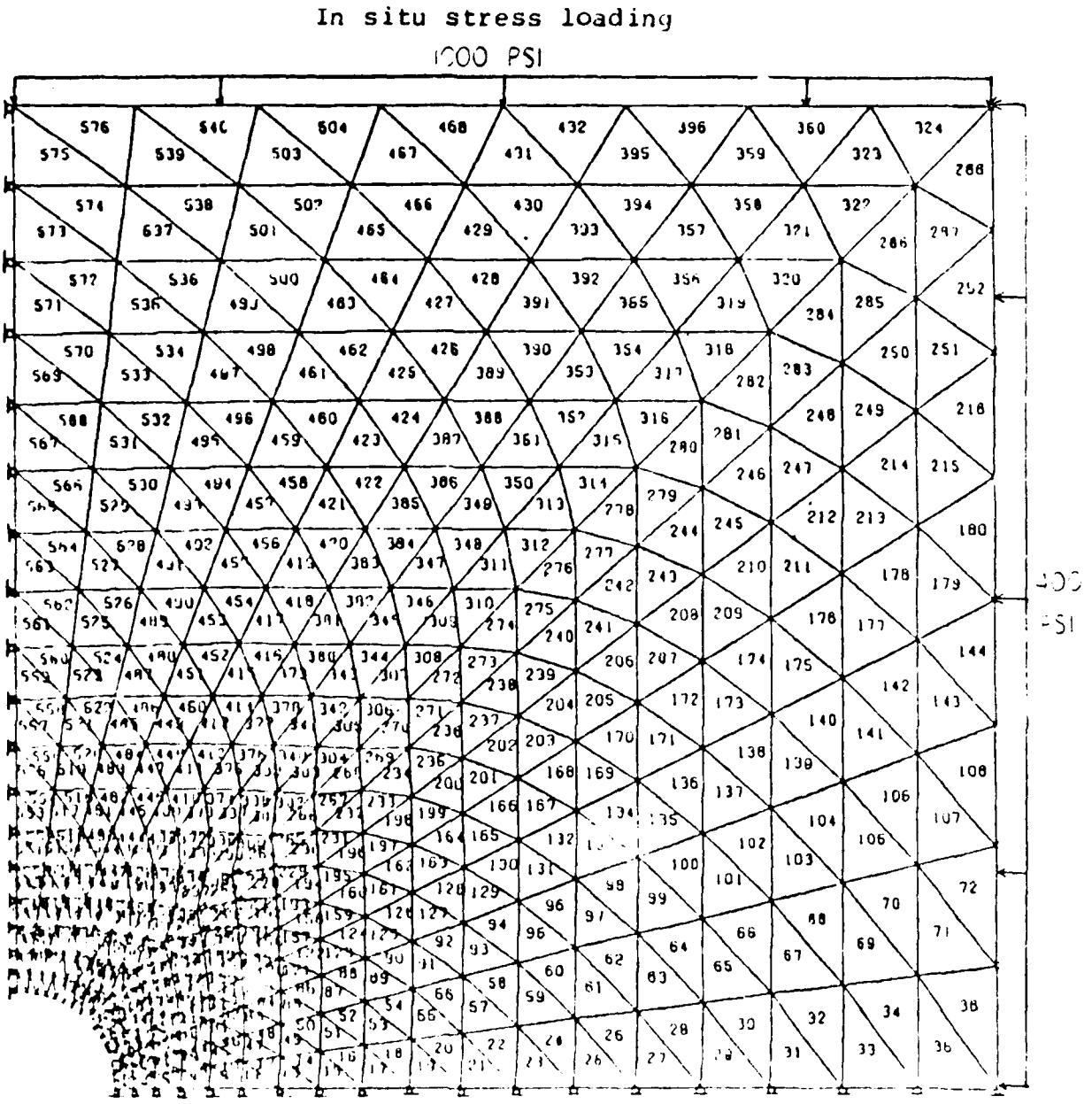

Fig 9. Finite Element Model: 323 Nodes, 576 Elements

VI. Program Verification

One-Dimensional

To verify the changes made in VISCO to employ the Drucker-Prager elastic-perfectly plastic material model, a one-dimensional viscoplastic analysis was done using a plane stress, simple tension, two-element model. Owen (Ref 5) notes that for this case, a stress unbalance will always exist and steady state conditions cannot be achieved using the initial strain approach of VISCO as would be expected. In equation form

$$\dot{\varepsilon}^{i}_{vp} = \gamma[\sigma^{i} - (\sigma_y + H\acute{\varepsilon}^{i}_{vp})] \tag{6.1}$$

but since $H' = 0$

$$\dot{\varepsilon}^{i}_{vp} = \gamma[\sigma^{i} - \sigma_y] \tag{6.2}$$

where $(\sigma^{i} - \sigma_y)$ is the stress unbalance. Using the algorithm described in Chapter III where stress strain relationships are in terms of the elastic stiffness, $\Delta\sigma$ or the increment of stress between time steps can be written in the following form:

$$\Delta\sigma = E(\Delta\varepsilon^{i} - \Delta\varepsilon^{i}_{vp}) \tag{6.3}$$

The two element case was run over a period of ten seconds and the stress increment approaches zero as it should so that response is contributed to the time interval size. For

$$\Delta\sigma = E(\Delta\varepsilon^{i} - \Delta\varepsilon^{i}_{vp}) = 0 \qquad (6.4)$$

or

$$\Delta\varepsilon^{i} - \Delta\varepsilon^{i}_{vp} \qquad (6.5)$$

Fig. 10 shows a delay in acquiring the zero $\Delta\sigma$ ($\Delta\varepsilon \neq \Delta\varepsilon_{vp}$). This can be attributed to the size of the time interval incorporated into the viscoplastic equation. The smaller the time step the closer the differential strains. The Visco model responded as indicated by Owen in that there is always a stress unbalance. Marcal (Ref 8) has shown that a time independent approach (non-visco) would produce a singularity for the same conditions.

Two-Dimensional

The Baker, et al (Ref 11) elastic-plastic tunnel analysis was used as another verification of the Drucker-Prager model used viscoplastically. Previous analysis showed that a stress concentration exists around the cutout when analyzed elastically. Note in Fig 11 the comparison between the σ_y stresses developed in the elastic solution and those developed in the elasto-plastic solution along a horizontal section through the tunnel. Steady state conditions were achieved using a fluidity parameter γ of 1.0 $in^2/lbf\text{-}sec$ Steady state is indicated by a zero strain rate (Eq 2.14) in all elements. The results illustrate the fundamental principle that plastic flow tends to relieve the high stress concentrations that would ordinarily develop in perfectly elastic materials. Because stresses are redistributed, note that the viscoplastic stresses exceed the elastic stresses as distance from the cutout increases. These

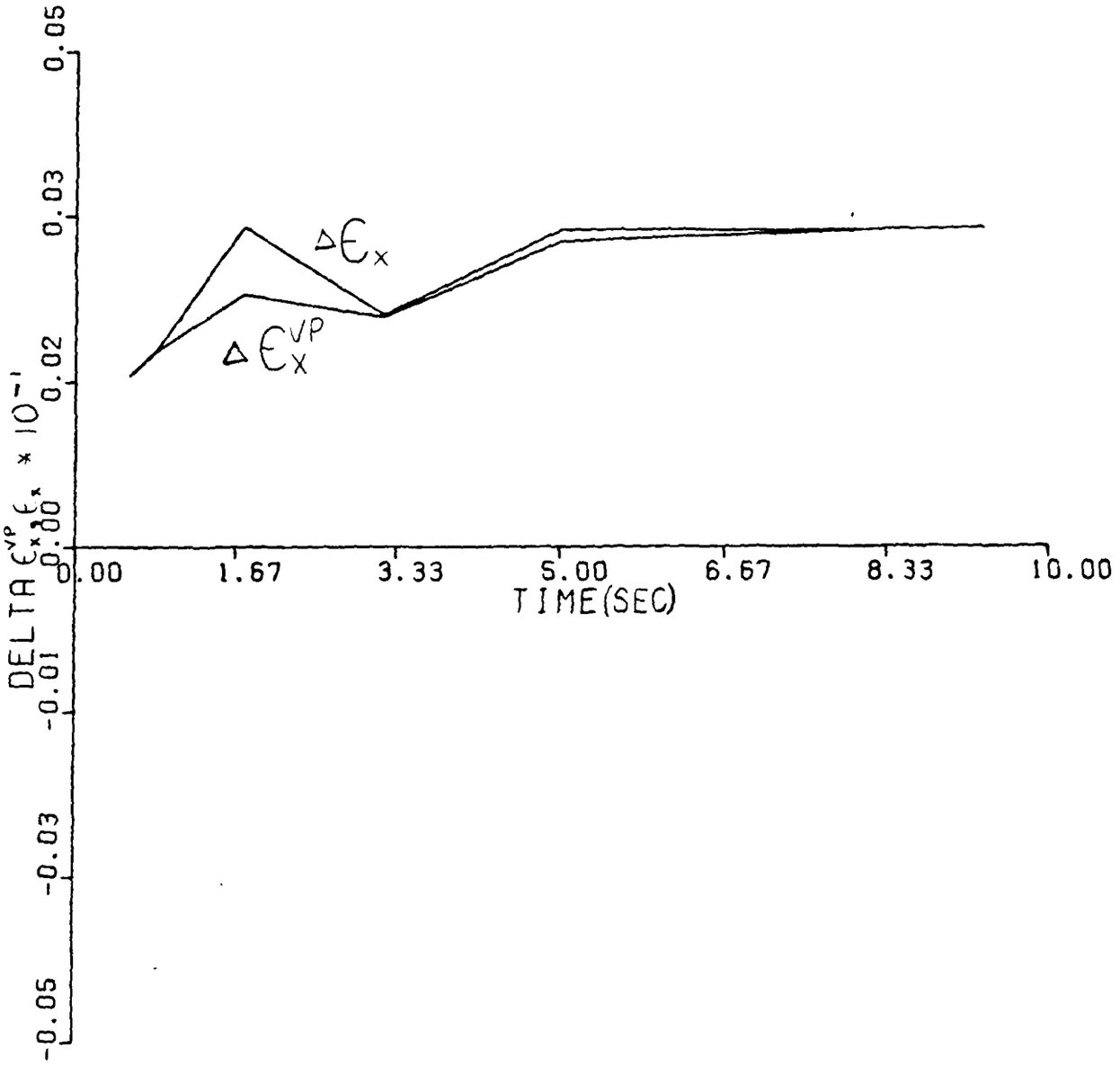

Fig 10. $\Delta\epsilon^i, \Delta\epsilon^i_{vp}$ vs. Time for the Two Element Model Under Uniaxial Tension

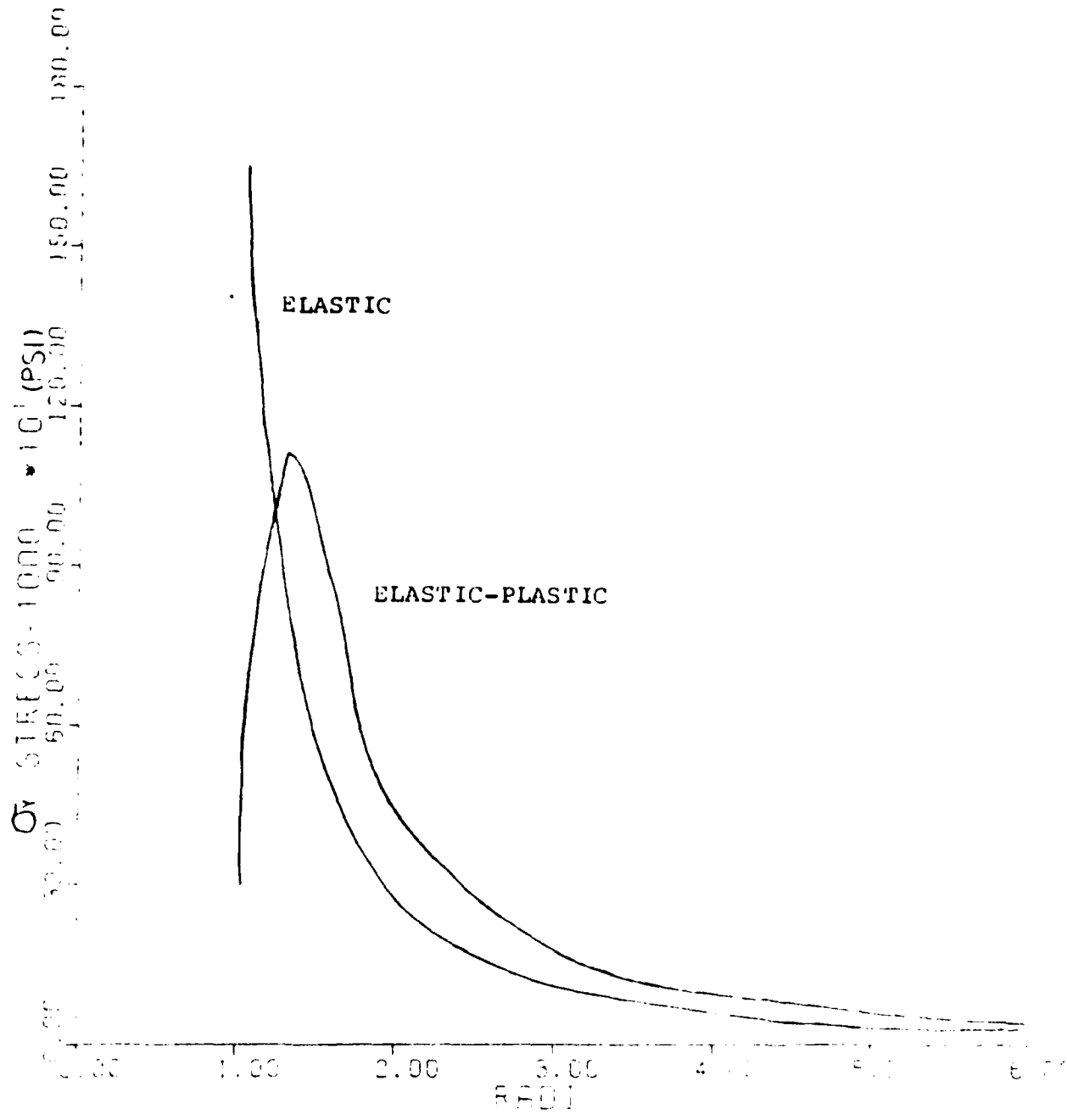

Fig 11. σ_y Comparison Between Elastic and Viscoplastic Solutions Under In Situ Loading

results compare well with Baker's; within 15% for σ_y and within 5% for σ_x .

Due to the high cost and lengthy computer time required for solution of the equilibrium equation when using the 576 element model, a new model was developed (Fig 12) containing only 238 elements. The 576 element model (fine mesh) required computer time (CPU time) of 700 seconds at a cost of $52.34 to solve Baker's elastic-plastic problem, while the 238 element model (course mesh) required 285 seconds at a cost of $20.38. A comparison between the two meshes in terms of stresses σ_x and σ_y along three representative radials is detailed in Figs 13-18; note that the two meshes do not vary by more than 10%. The accuracy developed by the coarser mesh versus its lower cost, dictated use of the model for the remainder of the study.

The final comparison designed to validate both program and model contrasts material movement generated experimentally (Ref 1) versus material movement predicted using the theory and model developed thus far. Using loads that approximate loading at tunnel levels from a nuclear blast, resulted in nodal displacements presented in Fig 19. Note that in the vertical direction, most material moves up away from the cutout while the node at the springline moves in the opposite direction because the cutout provides no support (all cutout nodes collapse inward). This compares excellently with experimental results.

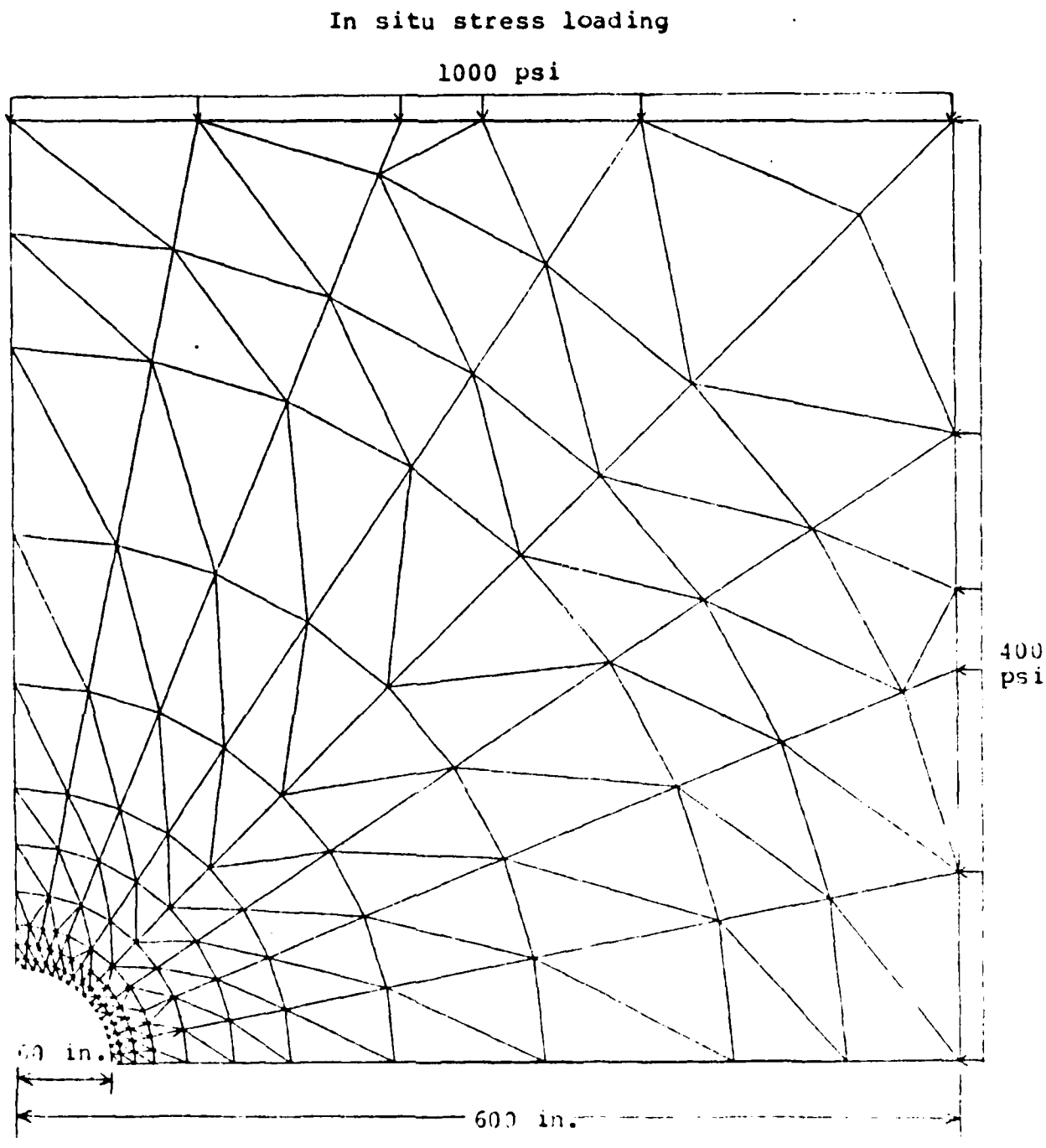

Fig 12. Finite Element Model: 144 Nodes, 238 Elements

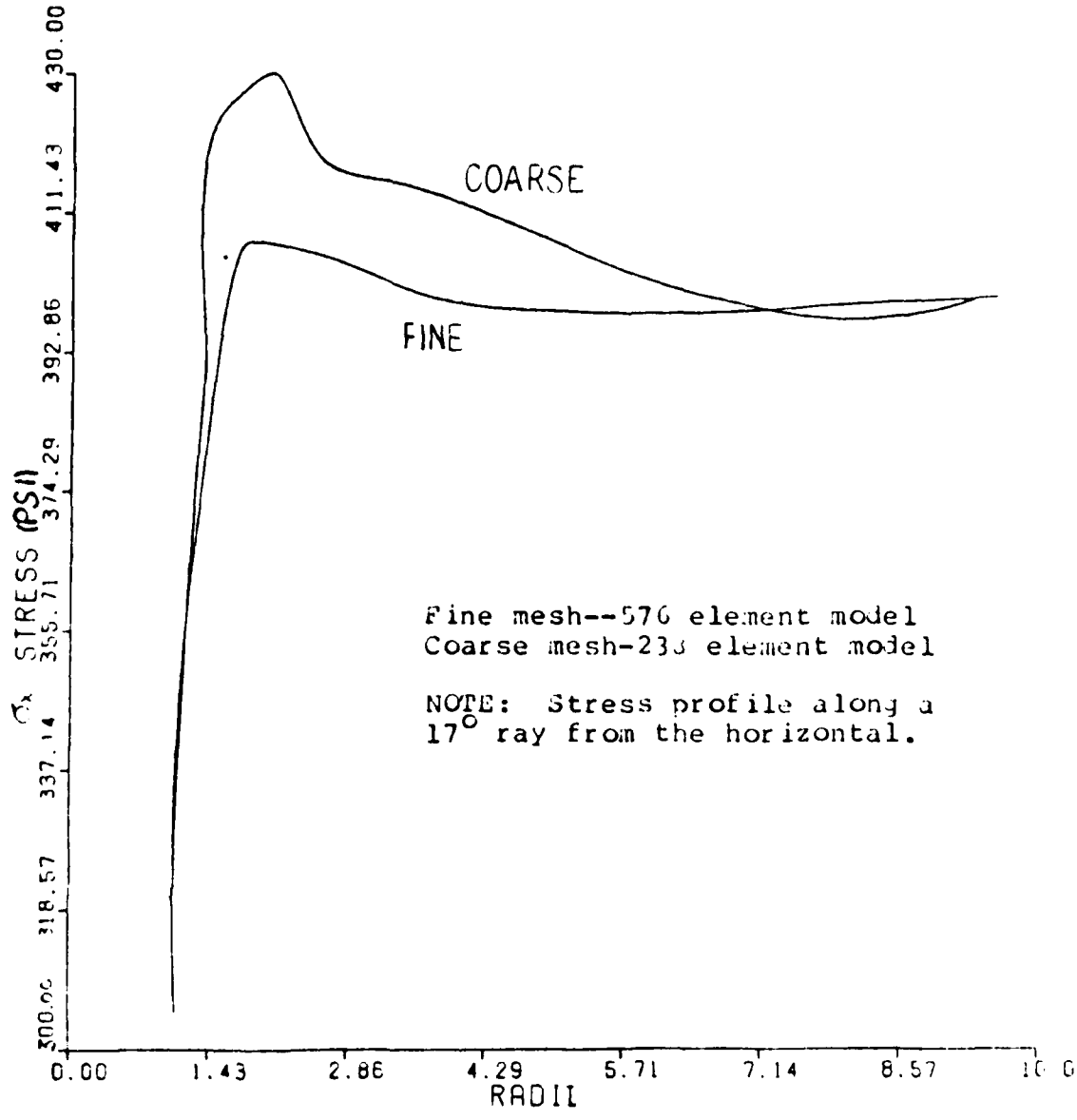

Fig 13. σ_x Stress Comparisons

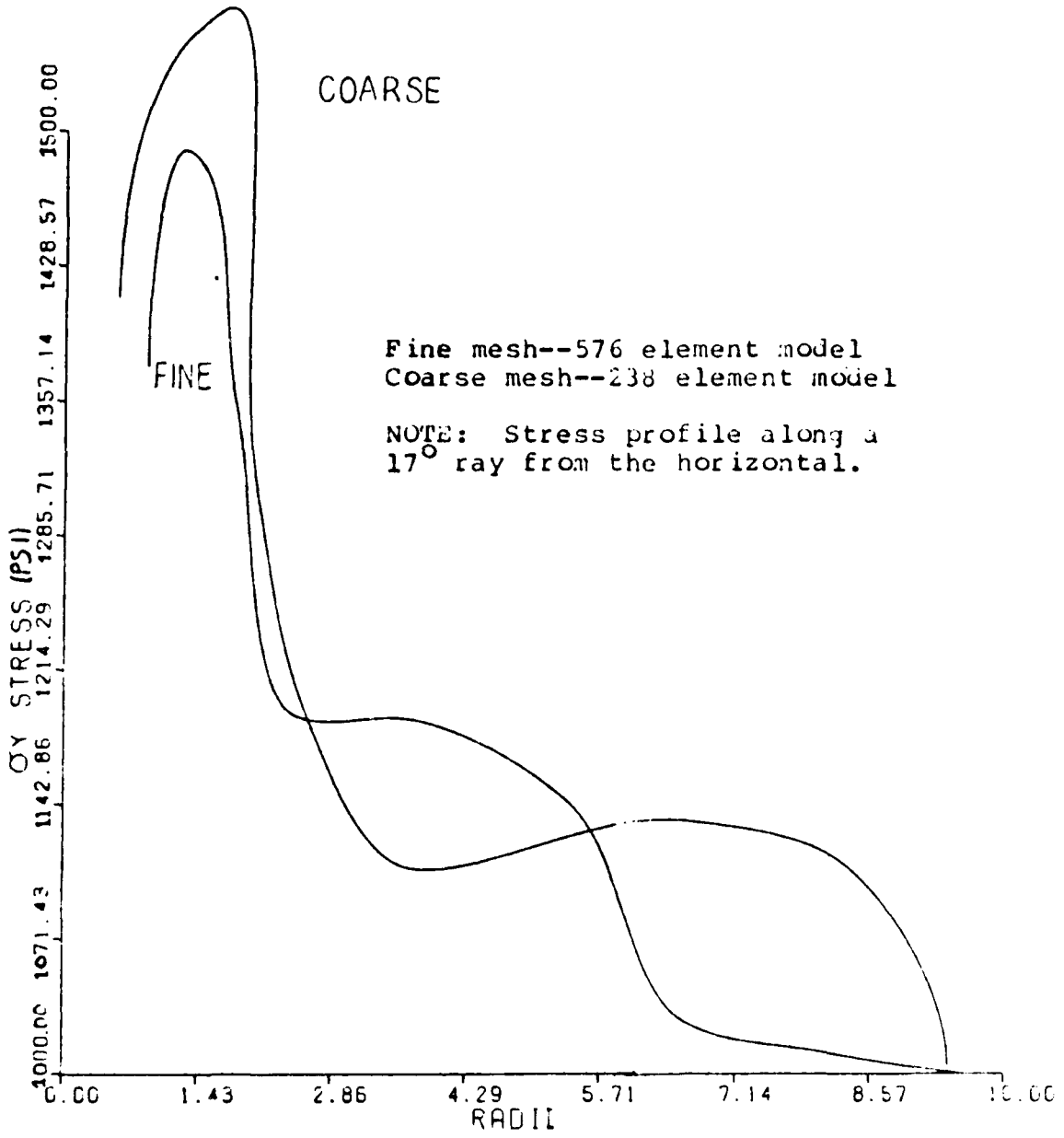

Fig 14. σ_Y Stress Comparisons

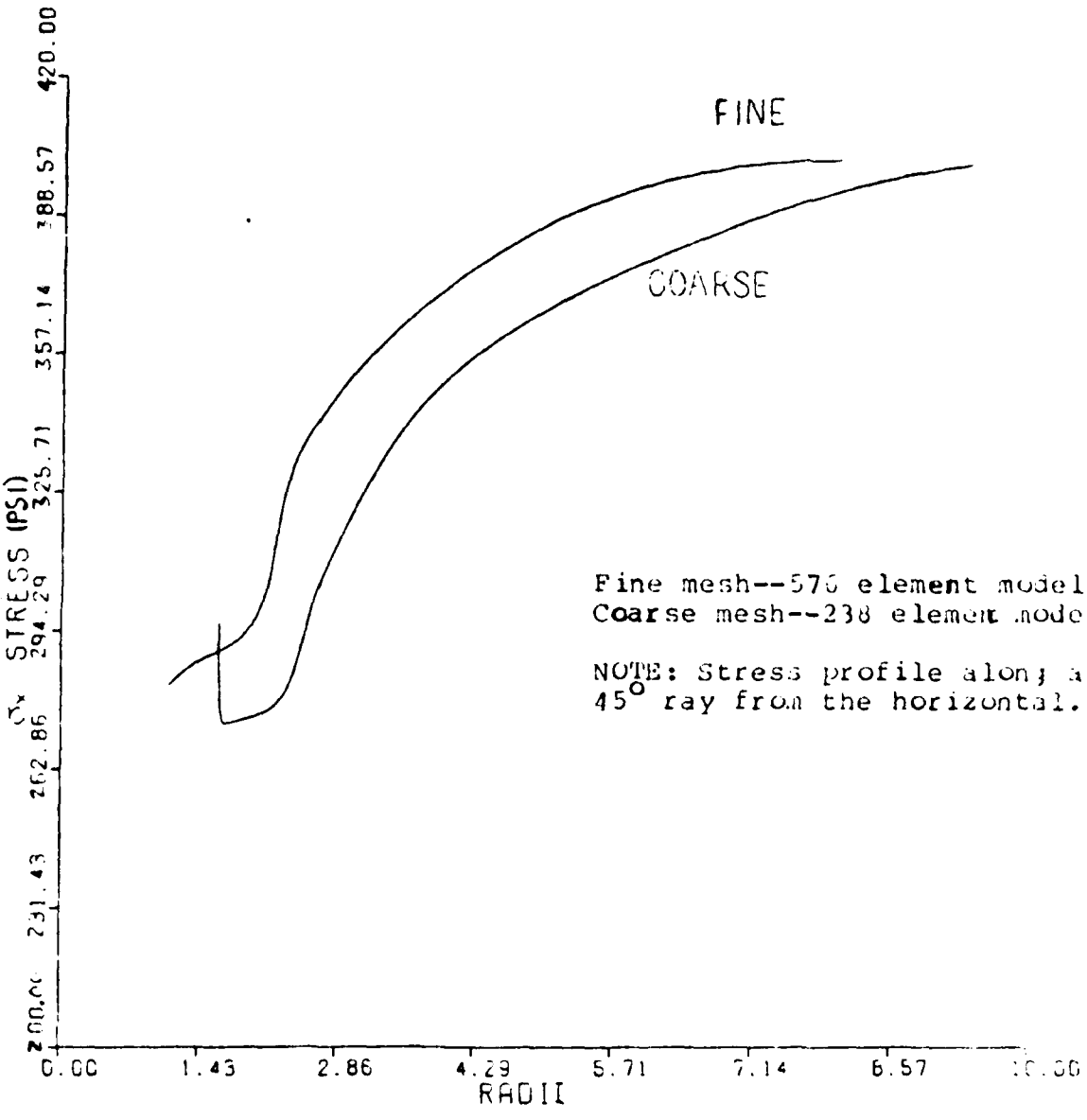

Fig 15. σ_x Stress Comparisons

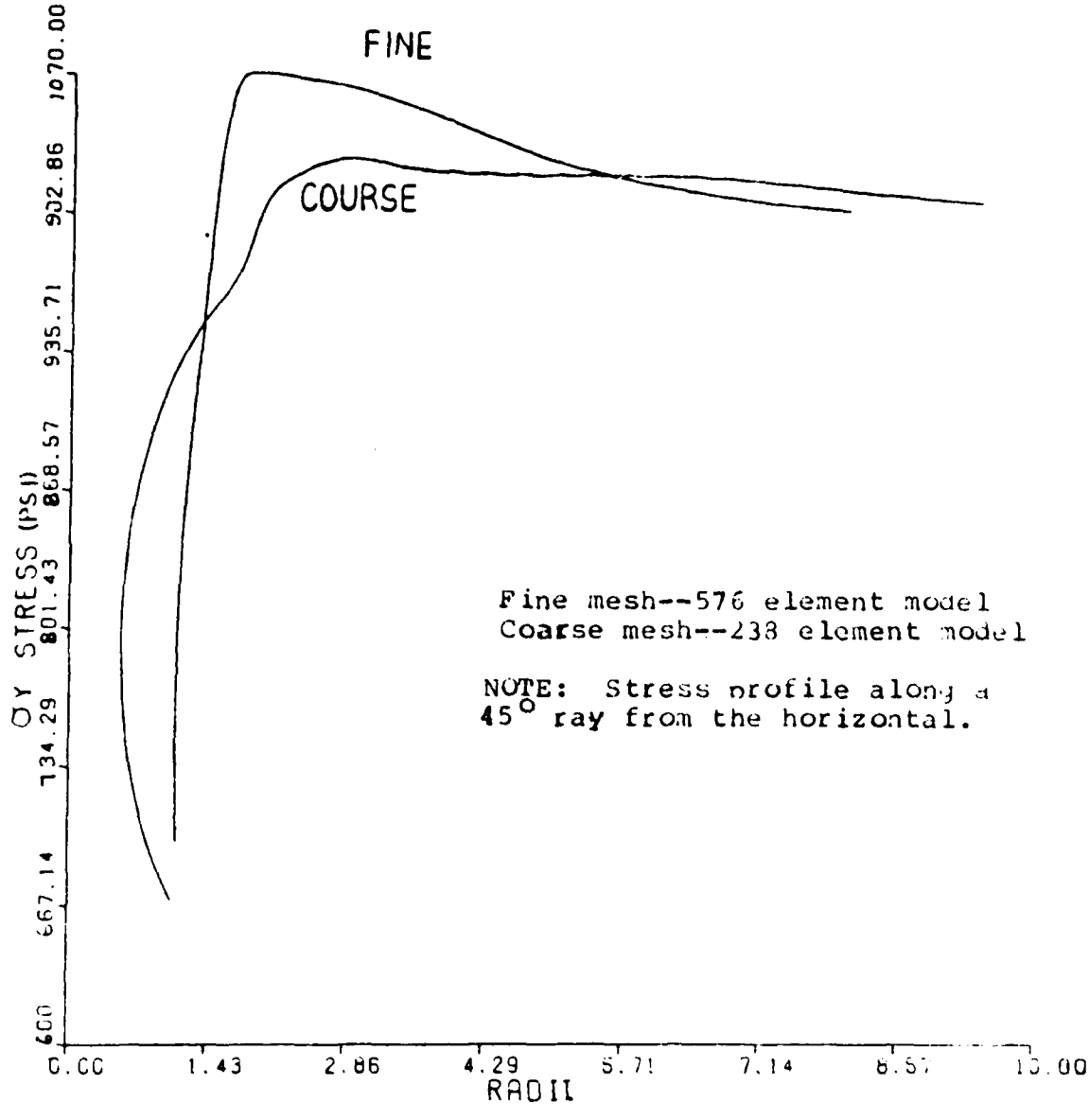

Fig 16. σ_y Stress Comparisons

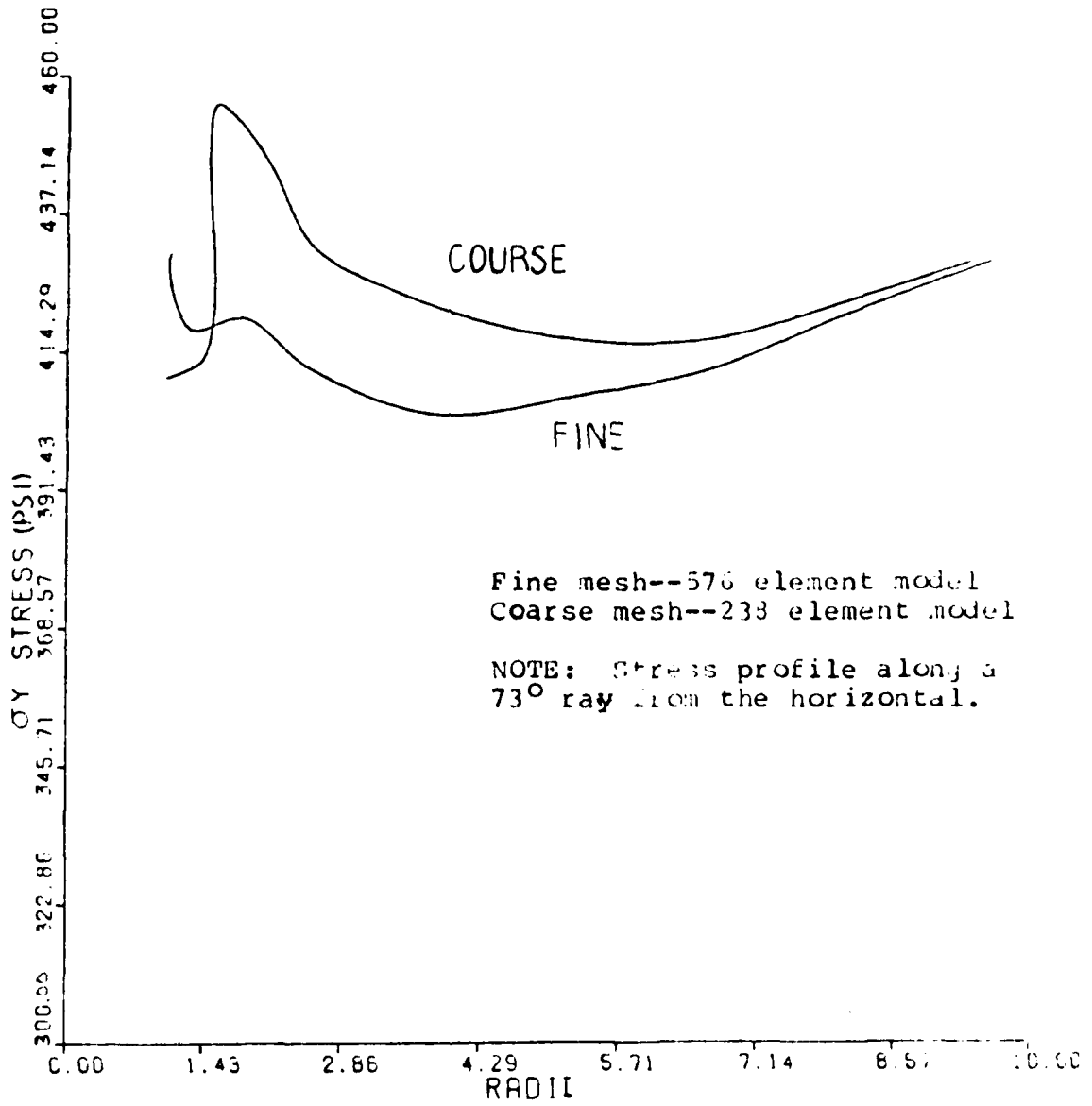

Fig 17. σ_x Stress Comparisons

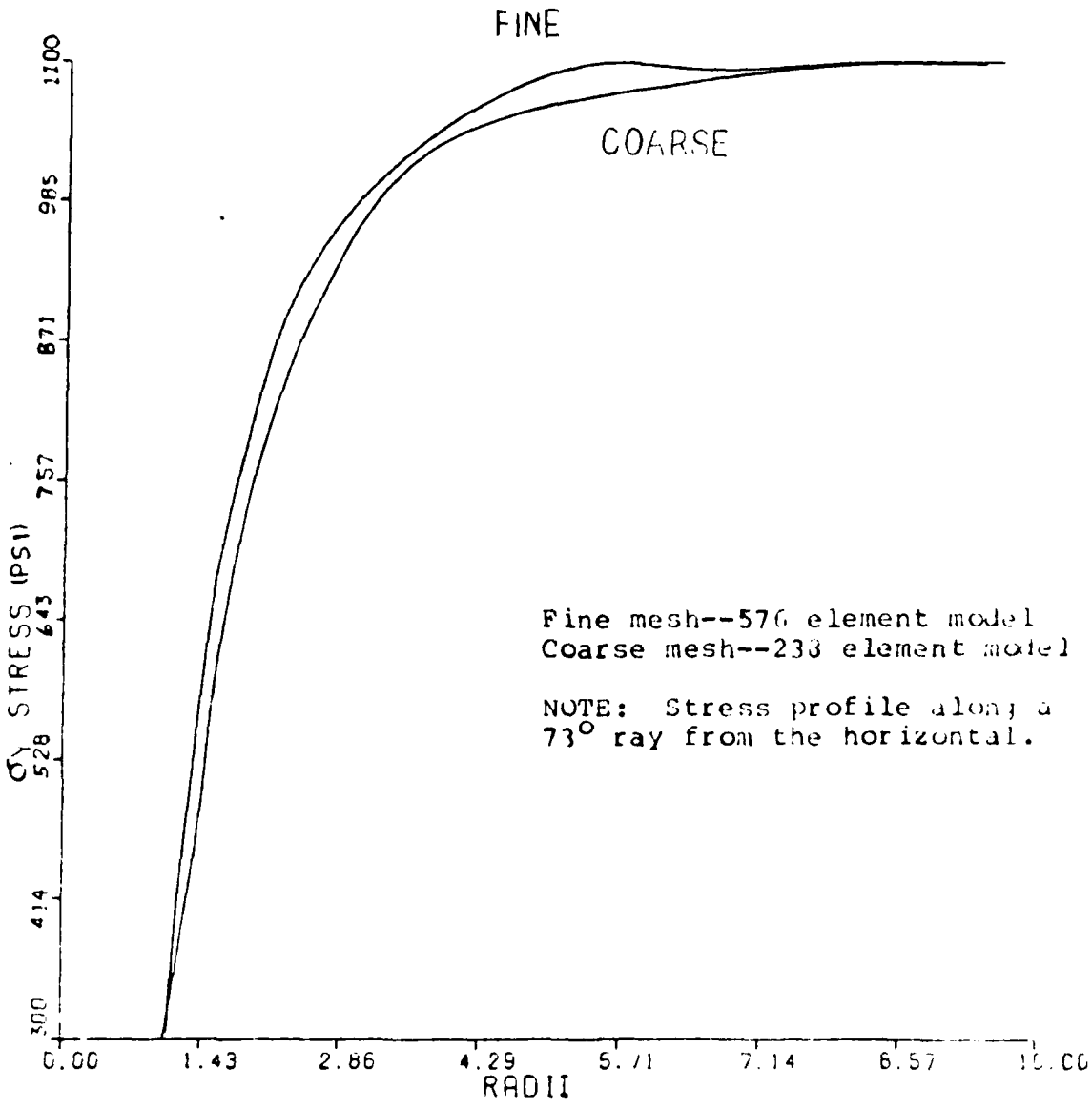

Fig 18. σ_y Stress Comparisons

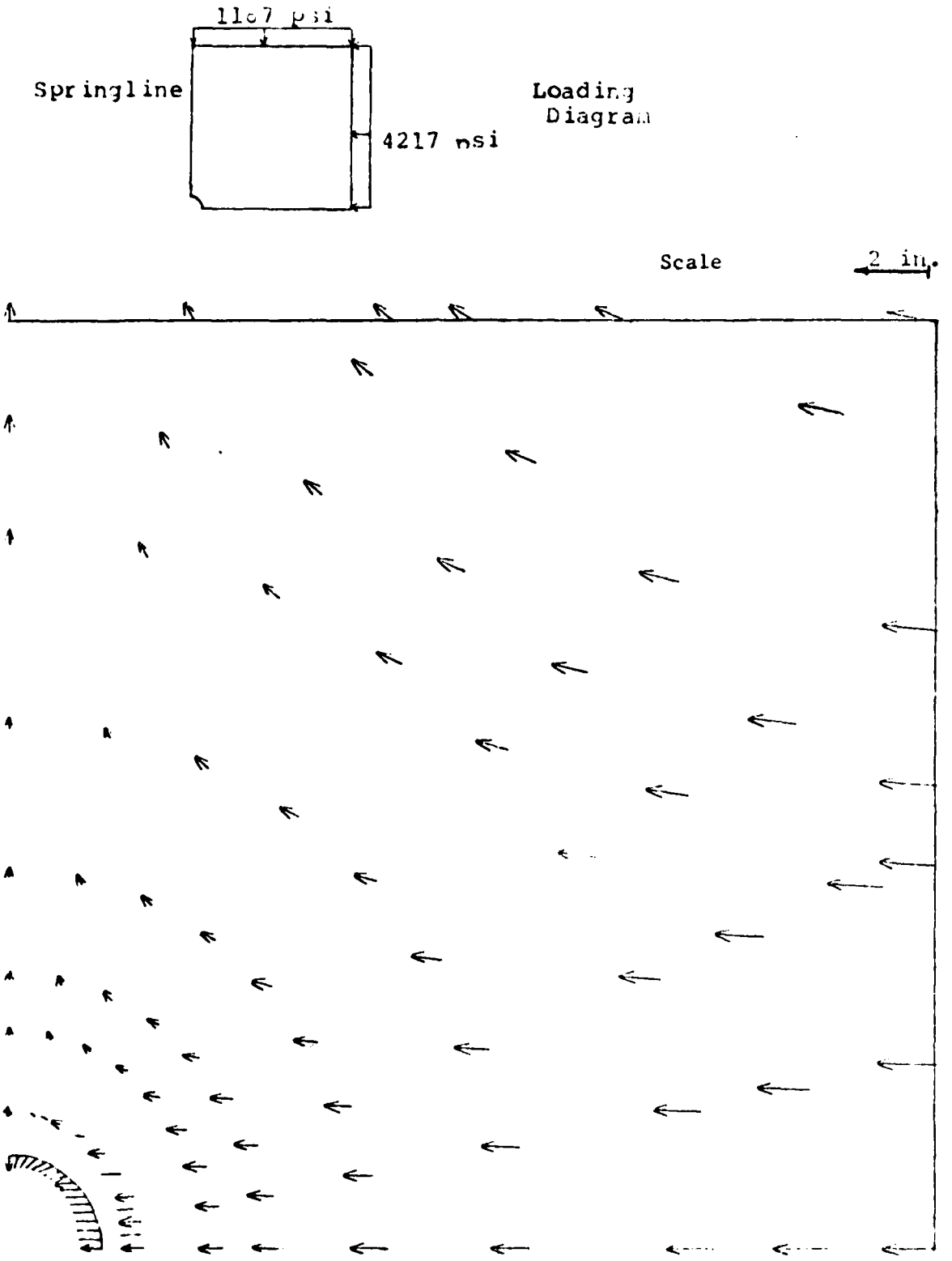

Fig 19. Model Nodal Displacements--1/4 kbar

VII. Results and Discussion

Quasi-Static Analysis

Two different loadings are considered in this section and in the following section, representing either varying nuclear weapon yields, varying tunnel depths, or both. In situ loads were also considered, and are merely added to the pressure wave loading. For convenience, the lower magnitude loading will be referred to as 1/4 kbar (1 kbar = 15,000 psi), the higher loading as 1/2 kbar loading. The weapons effect loading shown (Figs. 15, 16) can be attributed to wave propagation studies as indicated in Reference 1.

Figures 20 and 21 show the plastic zone developed for 1/4 and 1/2 kbar loading respectively, using a γ value of 1.0. The reader should recognize that even though a steady state solution is being carried out, a relatively small value for γ is being used. This value simply means that steady state is obtained after a longer period of time compared to larger γ's . Note that the plastic zone envelopes the entire cutout for the larger load and that the vertical applied stress (3475 psi) for this larger load has increased in greater proportion than the horizontal stress between the two cases. Figures 22 and 23 display tunnel deformation for the 1/4 and 1/2 kbar cases respectively. It can be seen that the 1/2 kbar case experiences much larger deformations than the 1/4 kbar case. Also note that the major deflection occurs at the crown for the 1/4 kbar loading, and at the springline for the 1/2 kbar

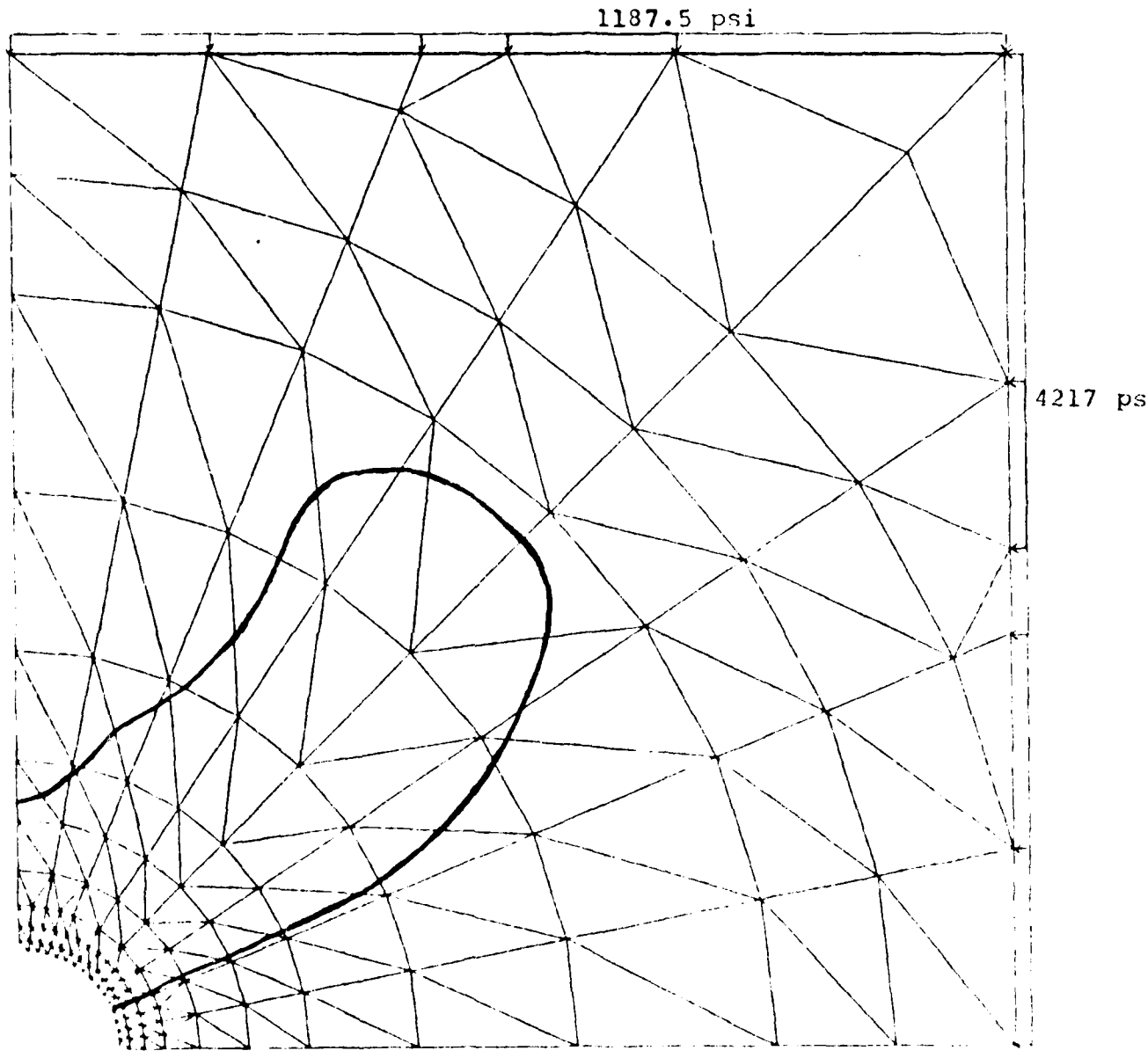

Fig 20. Steady State Plastic Zone--1/4 Kbar

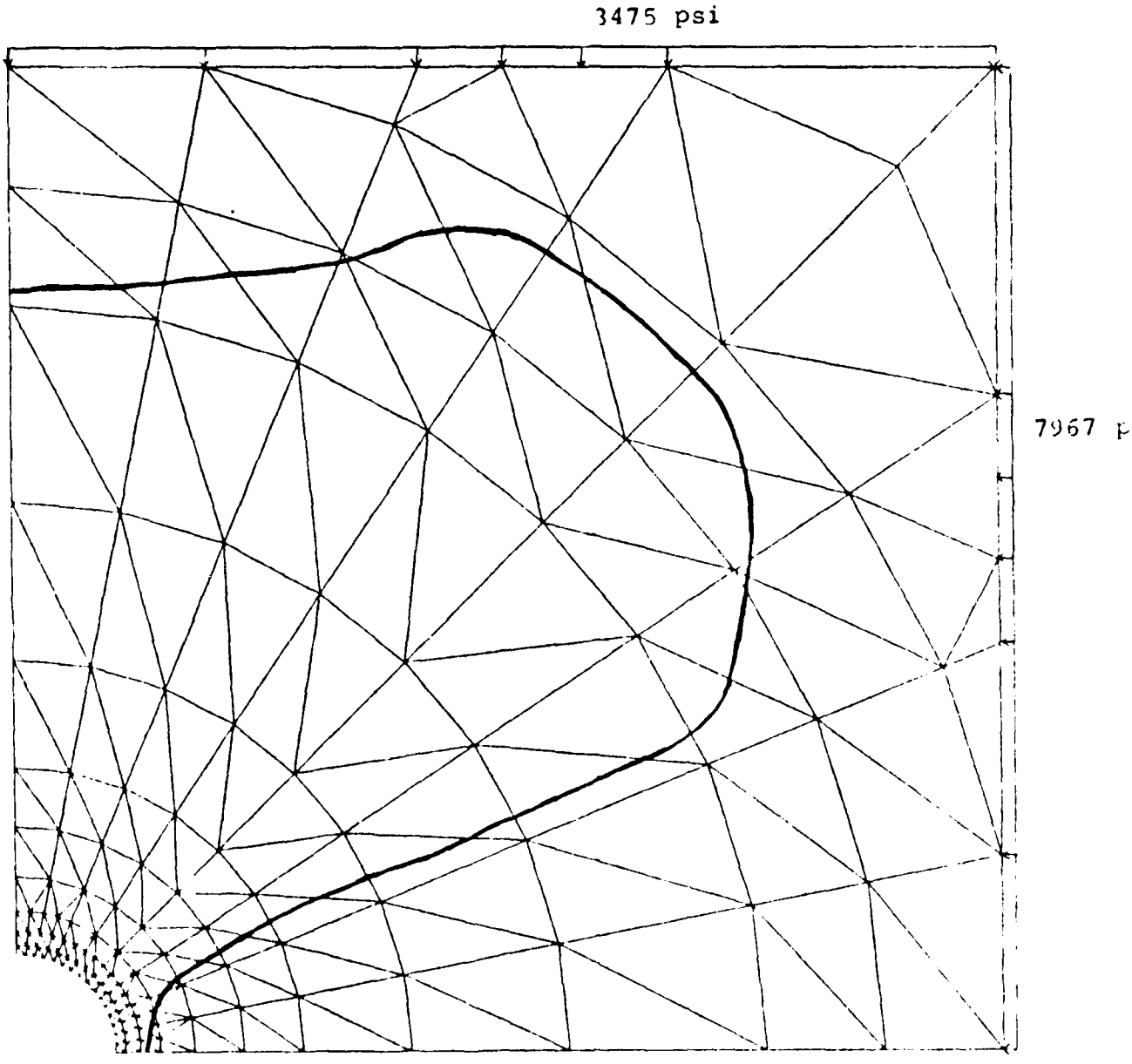

Fig 21. Steady State Plastic Zone--1/2 kbar

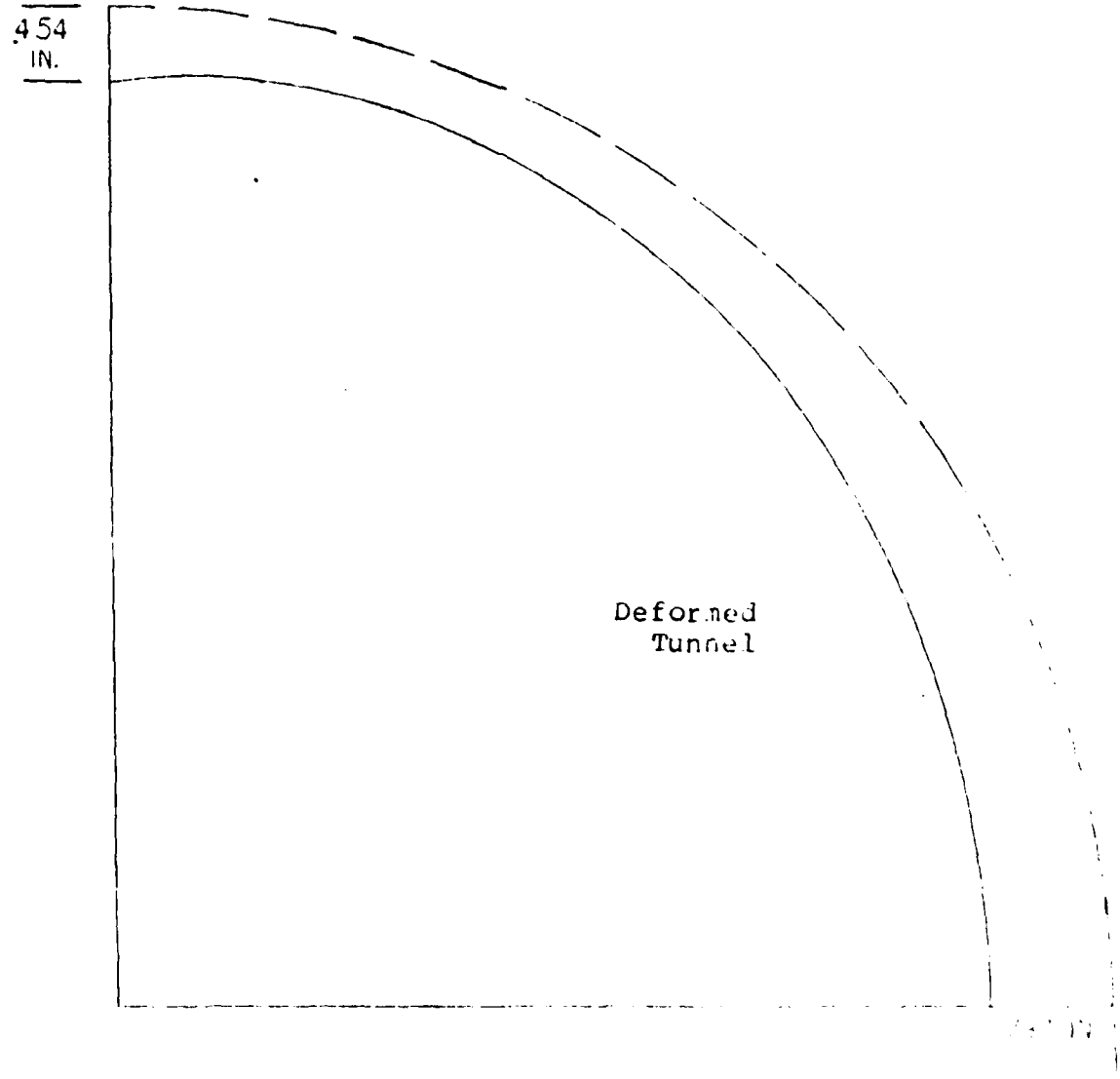

Fig 22. Tunnel Deformation--1/4 Kbar

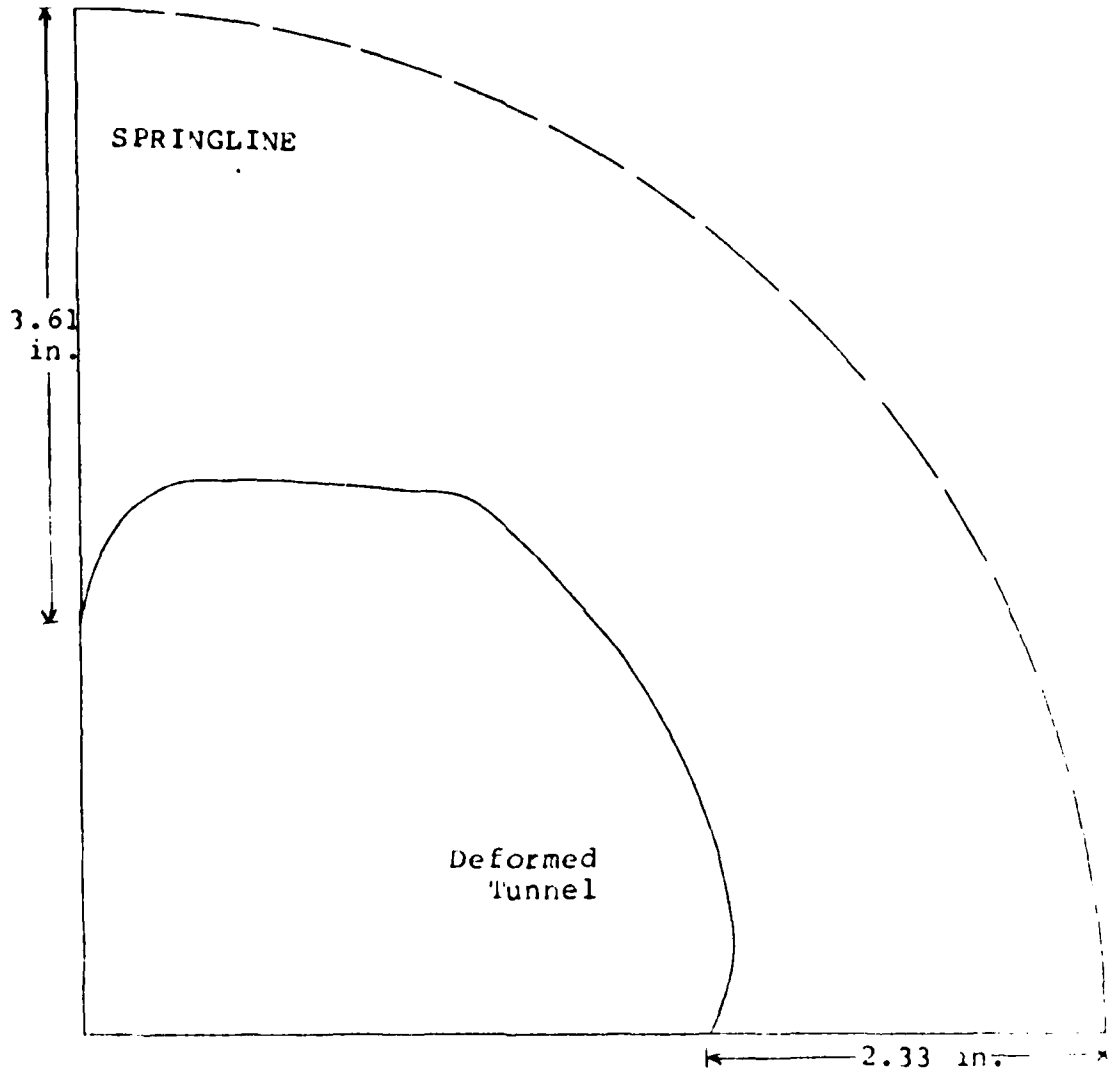

Fig 23. Tunnel Deformation--1/2 kbar

case. The much larger deformations for the 1/2 kbar loading are due to both the increased load and the fact that the entire tunnel is experiencing plastic deformation. Figure 19 shows nodal displacements in the model for the 1/4 kbar case; displacements are similar for 1/2 kbar loading (Fig 24). Both show springline area displacements consistent with experimentation (Ref 1).

Figure 25 compares plastic zone stresses along a 45° radial between the two cases, where positive values denote compression. The effective stress $\bar{\sigma}$ for all elements in the plastic region is the same (976.4 psi), despite the much larger stresses experienced for 1/2 kbar loading. It was noted earlier that plastic flow redistributes high stress concentrations. This redistribution of stresses is clearly seen here because the much larger stresses developed in the 1/2 kbar case versus the 1/4 kbar case still produce an effective stress equal to the constant yield stress k'. Note the variance in nodal displacements displayed in Figures 19 and 24. Because the Drucker-Prager yield criterion accounts for hydrostatic stresses (compressibility), a large amount of material movement through compaction and crushing occurs. Thus, the effective stress equals the yield stress for two reasons: relative displacements are not as large as they initially appear, and the model will only allow the effective stress to equal the yield stress in the plastic zone for steady state conditions (contrasting the results obtained below).

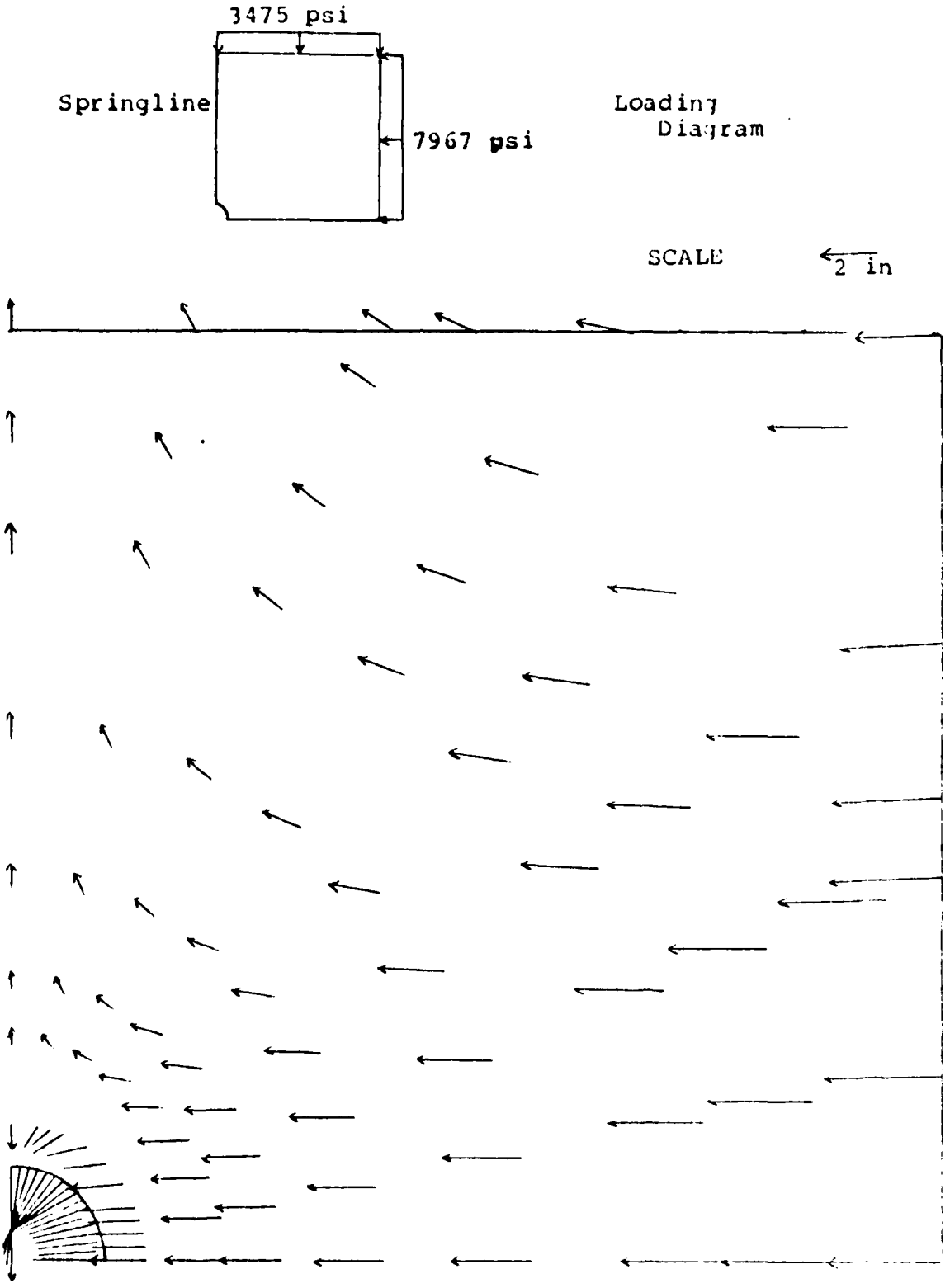

Fig 24. Model Nodal Displacements--1/2 kbar

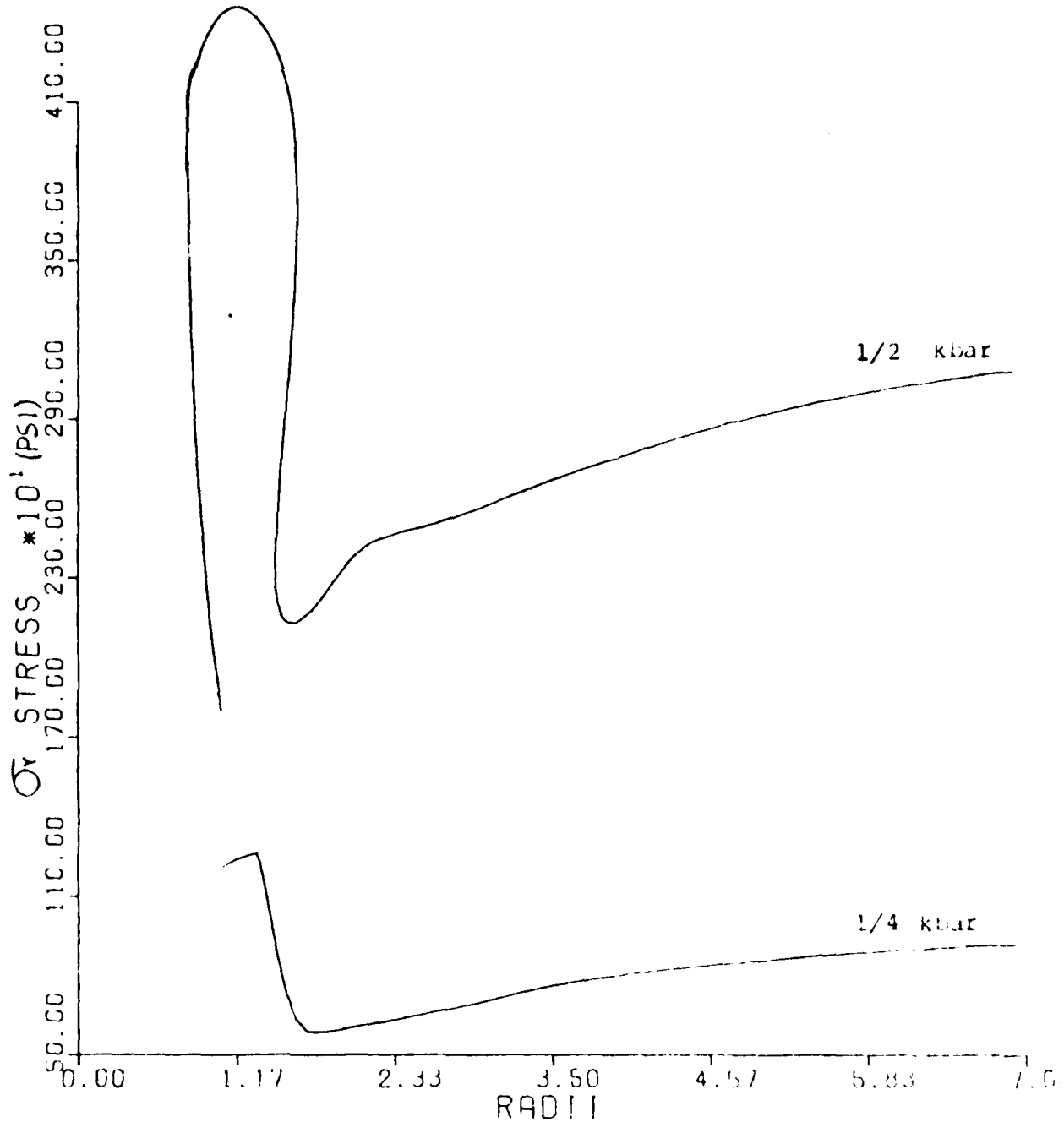

Fig 25. Plastic Zone J_y Stresses Along 45° Radial

However, this yield stress does not correspond to a unique strain level, as shown in Figures 26 and 27 which display effective plastic strain (Eq 3.2 below) contours in the plastic zone for the 1/4 kbar case and the 1/2 kbar case respectively. The larger effective strains in the 1/2 kbar case (at least 6 times greater) indicate more straining occurring, which explains that case's larger plastic zone.

Twenty-four elements in the 1/2 kbar loading model experienced tension in one or both component directions (x or y). These elements were all within 27 inches of the cutout and on radials from 11° to 90° from the horizontal (note that Fig 25 shows no tension because plotted stresses are averaged between two adjacent elements and compression always dominated tension). However, 9 of the 24 tension elements were concentrated between the 85° and 90° radials. This concentration of tensile stresses is appropriate when viewed in terms of material movement at the springline depicted in Fig 24. The 1/4 kbar case also had tension elements, although fewer and confined to radials from 75° to 85°. Comparing the two cases, strain components, as well as effective strains, were on the order of 4 to 5 times larger for tension elements in the 1/2 kbar cases versus 1/4 kbar. Strains this large could be indicative of tensile material failure.

Quasi-Transient Analysis

In order to more accurately represent the physical wave propagation through the tunnel, a triangular loading function

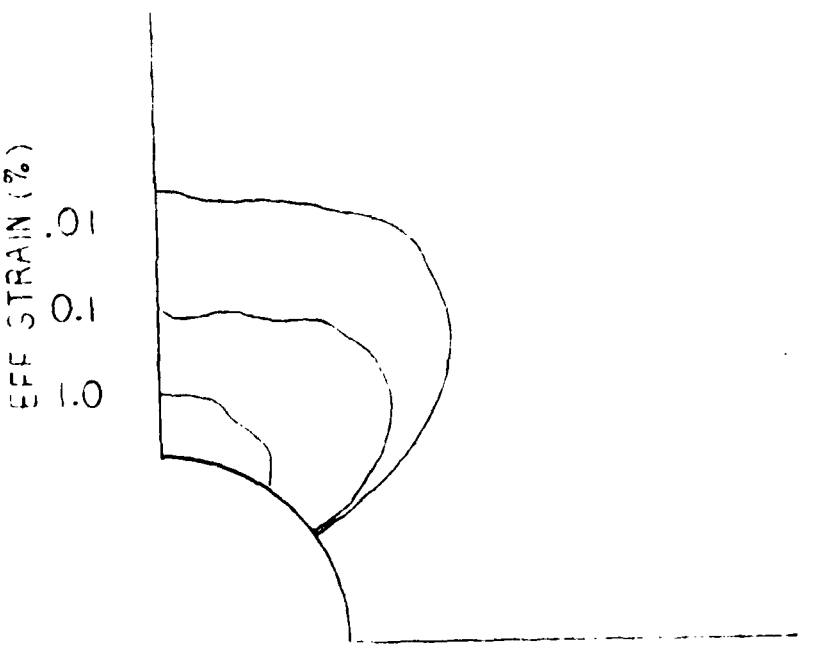

Fig 26. Effective Plastic Strain Profiles--1/4 Bar

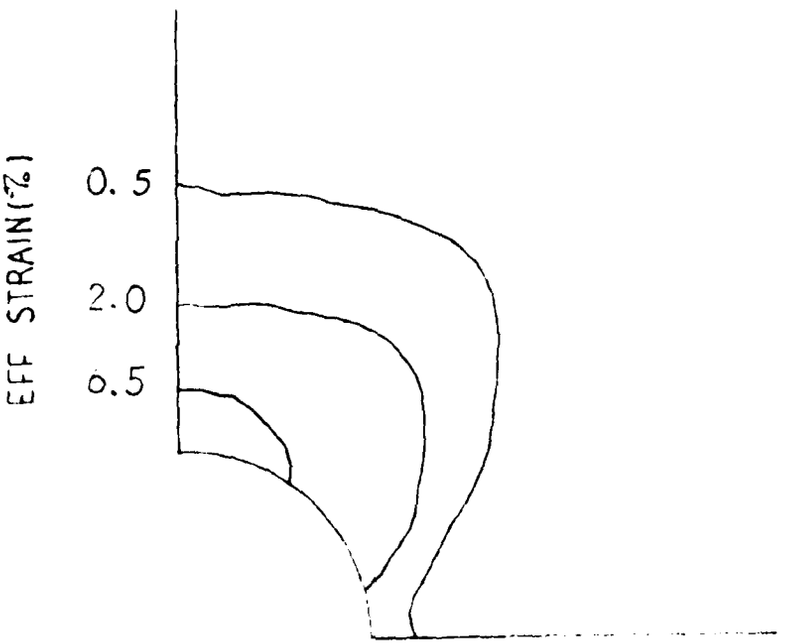

Fig 27. Effective Plastic Strain Profiles--1/2 kbar

(as indicated in Ref 1) was incorporated into the analysis. Two different load rates (supplied by the sponsor) were used, which are a function of the loading levels.

Figures 28-31 show plastic zone development for quasi-transient loading. Note the differing values of the fluidity parameter γ (0.1 and 1.0) chosen to provide a lower and upper bound for possible γ values to be determined experimentally. Recall that $\gamma = 1.0$ was used in the steady state analysis. The same γ value is now being used to study a transient state. This can occur due to the unique set of equations present in the viscoplastic solution. As employed here, γ is truly acting as a time dependent function, rather than as a so called dummy variable as it was in the steady state approach. Each figure shows the load history; P_{min} vertical (1000 psi in situ load) does not equal P_{min} horizontal (467 psi in situ load). Loads shown are maximum loads (in situ plus weapons effect). Comparison with the static results (Figs 20, 21) reveal significantly smaller plastic zones for both load levels, because the short times modeled do not allow as much plastic flow as in the steady state analysis. The size of the 1/4 kbar transient plastic zone was 27% and 47% of the static plastic zone for $\gamma = 0.1$ and $\gamma = 1.0$ respectively. For the 1/2 kbar case, 15% and 43% of the static plastic zone for $\gamma = 0.1$ and $\gamma = 1.0$ respectively. The plastic zones for $\gamma = 1.0$ (Figs 29, 31) are larger than the zones for $\gamma = 0.1$ (Figs 28, 30) because $\gamma = 0.1$ provides less plastic flow as dictated by Eq (2.14).

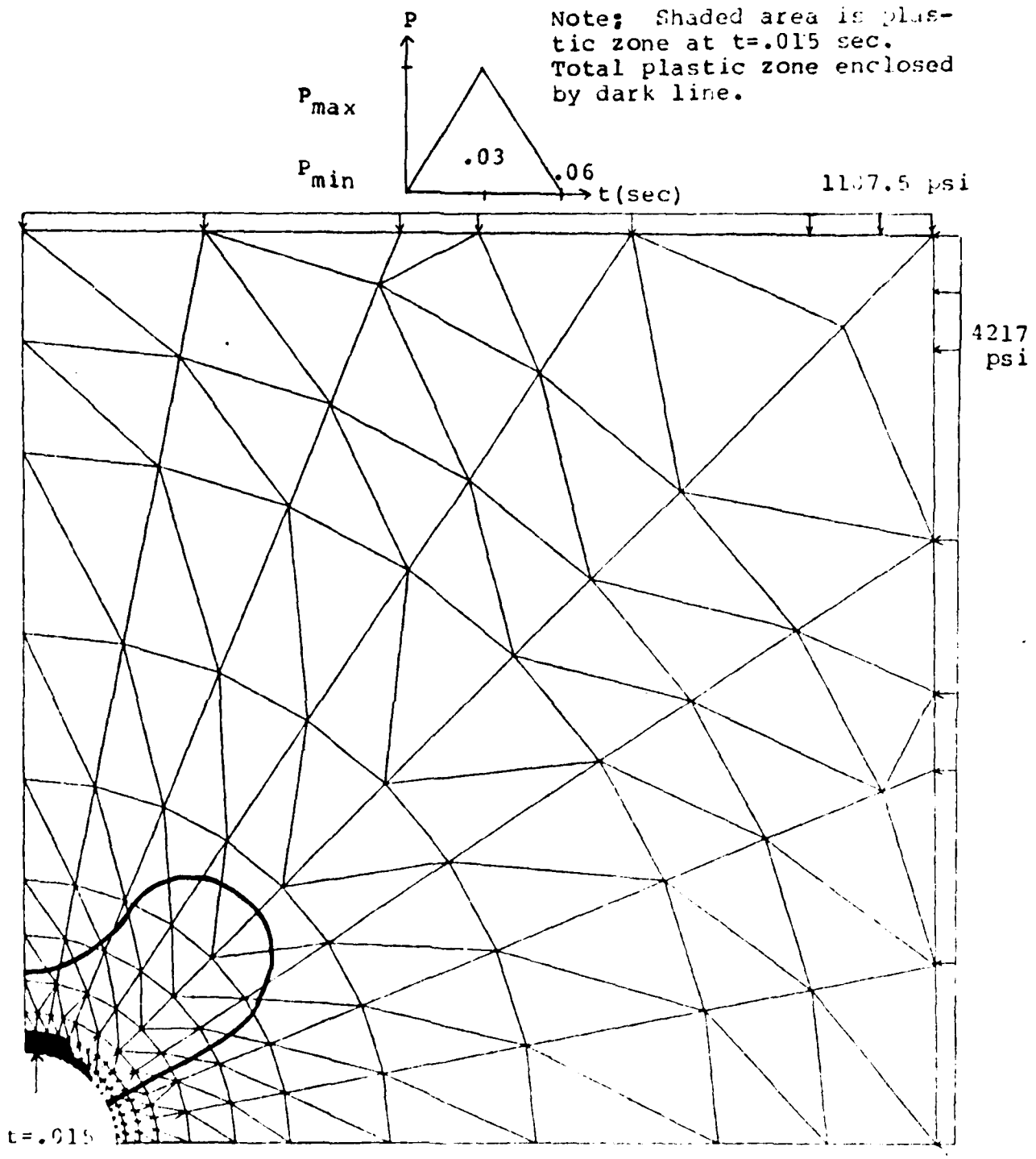

Fig 28. Transient Plastic Zone--1/4 Kbar, $\gamma = 0.1$

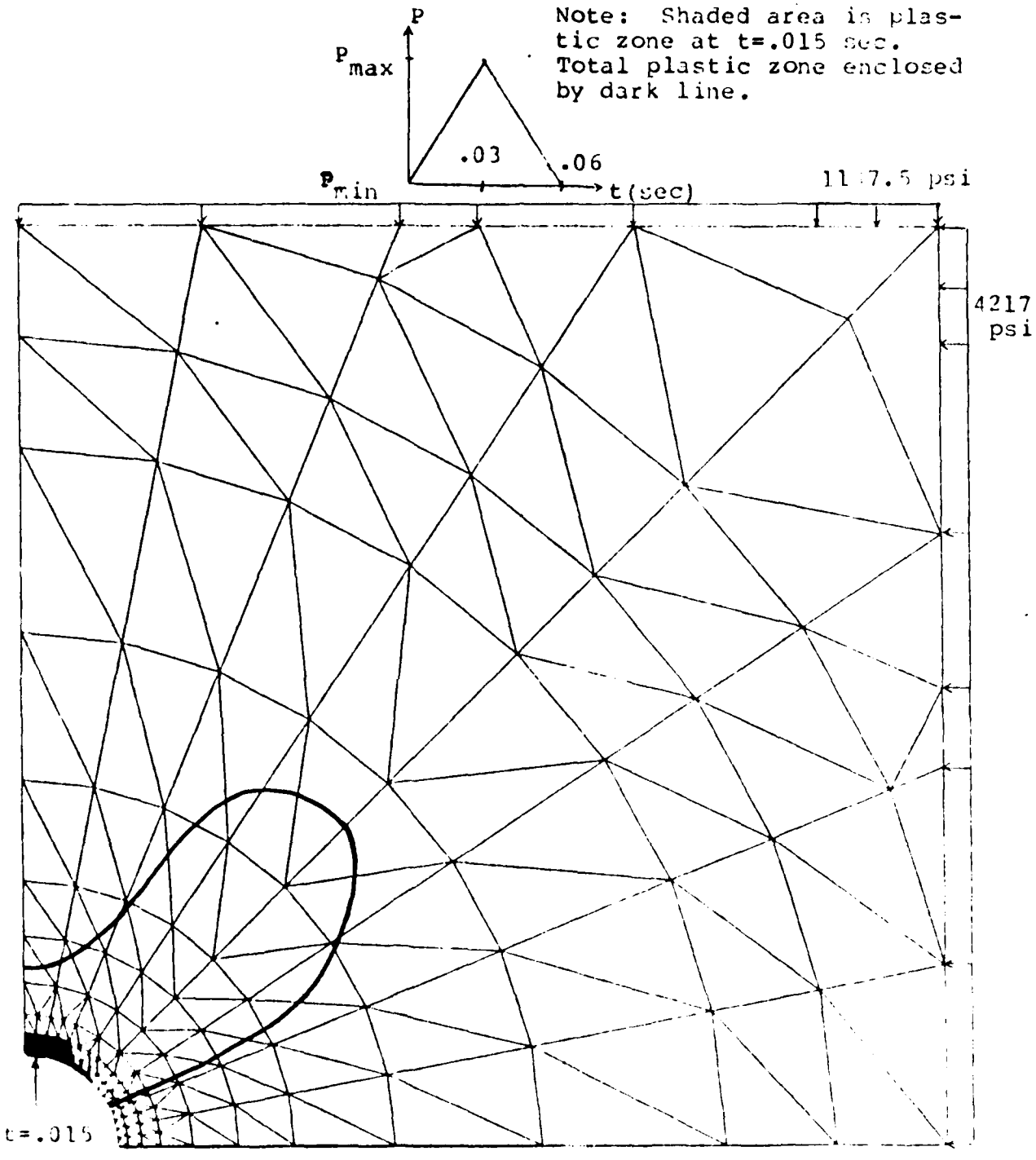

Fig 29. Transient Plastic Zone--1/4 kbar, . = 1.0

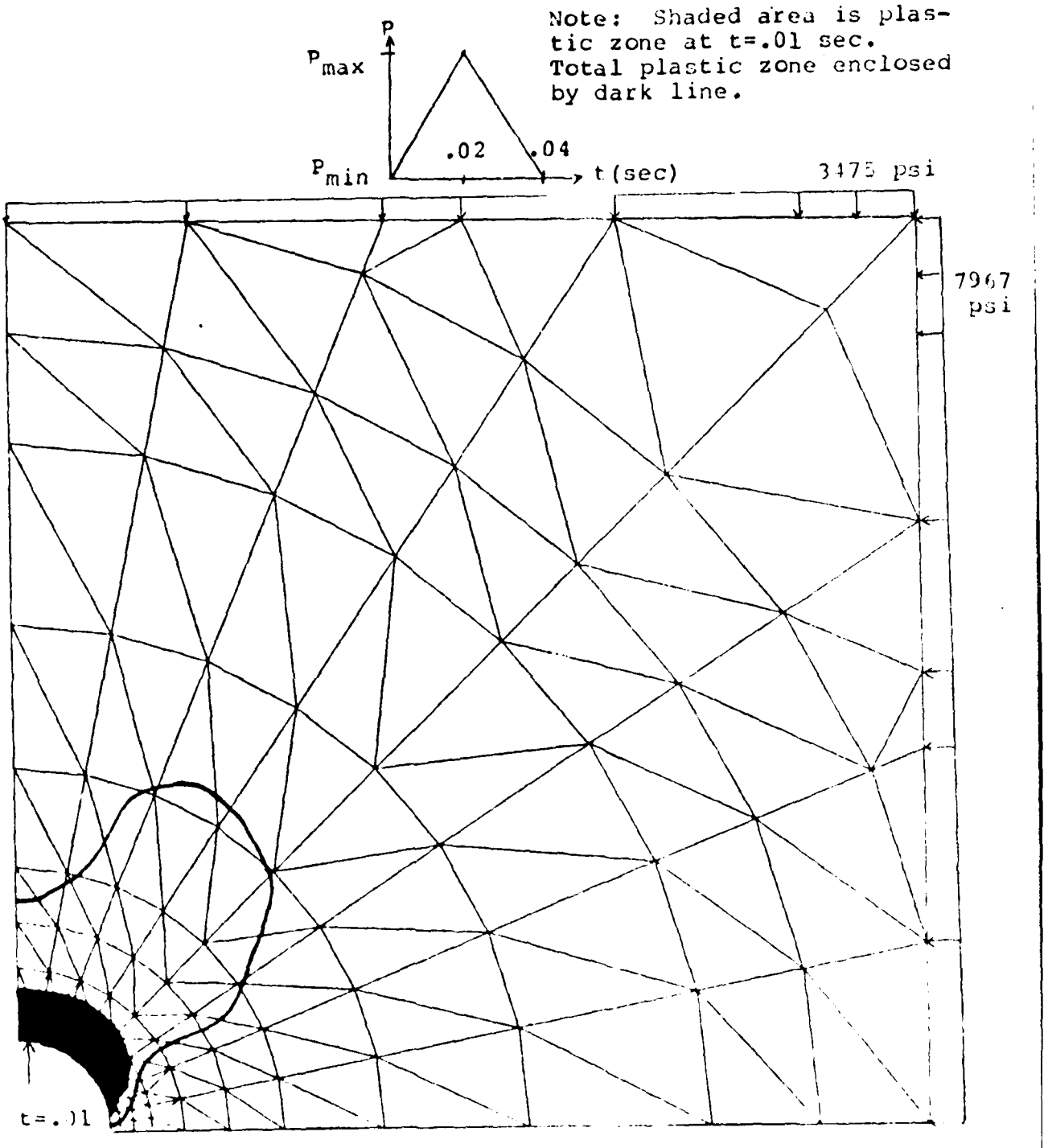

Fig 30. Transient Plastic Zone--1/2 kbar, ν = 0.1

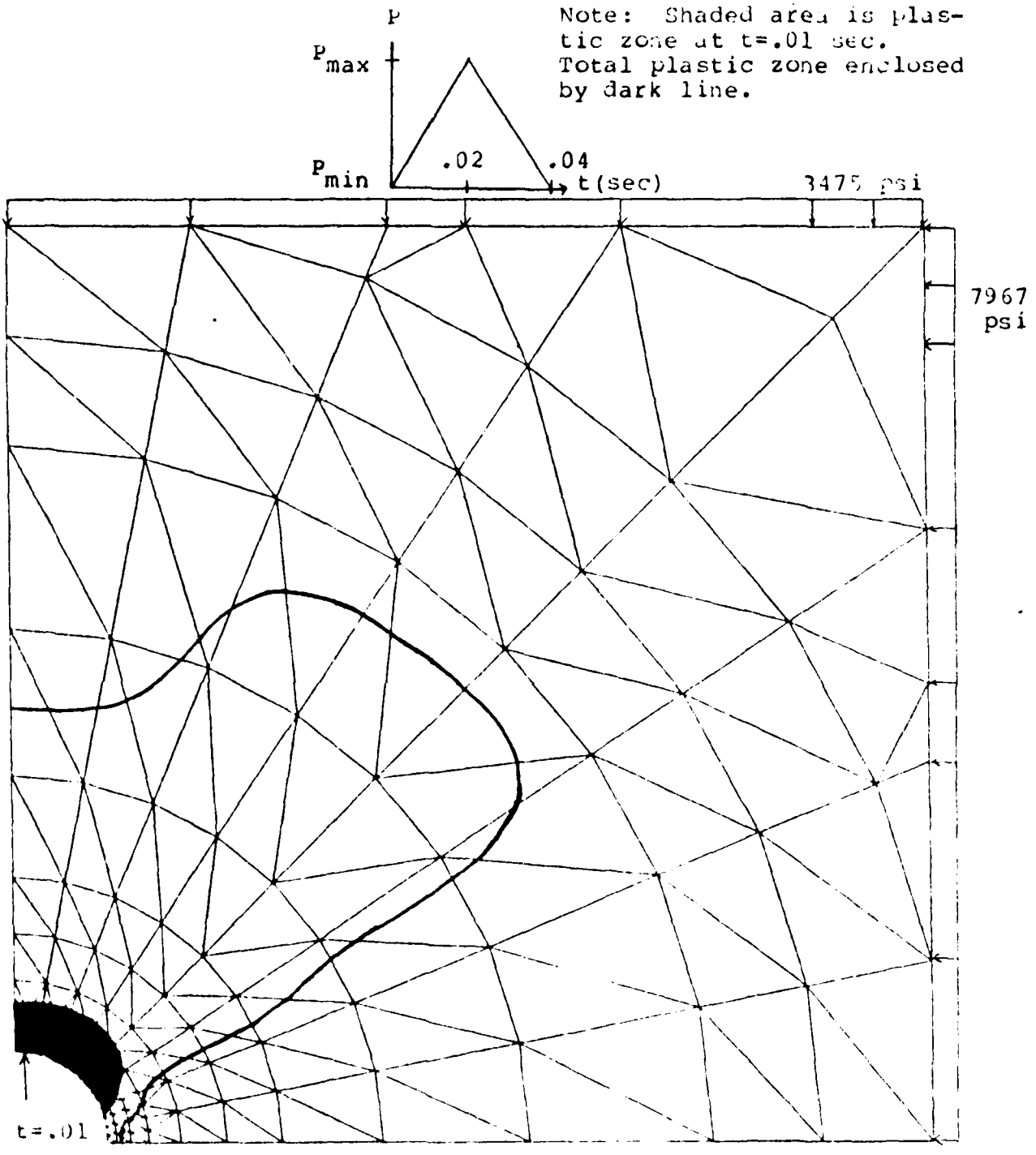

Fig 31. Transient Plastic Zone--1/2 kbar, γ = 1.0

Recall that viscoplastic material behavior as modeled by the one-dimensional rheological model (Fig 4) allows the stress level to instantaneously exceed the yield stress due to the overstress model employed. Effective stresses $\bar{\sigma}$ greater than the yield stress are shown in Figs 32 and 33, which are plots of $\bar{\sigma}$ versus time for an element in the plastic zone. Note the stresses in the 1/2 kbar case are roughly twice those in the 1/4 kbar case; both figures reflect a higher $\bar{\sigma}$ for $\gamma = 0.1$ because $\gamma = 1.0$ allows more plastic flow and thus lower stress. This larger amount of plastic flow ($\gamma = 1.0$) is also responsible for a larger final $\bar{\sigma}$ at $t = .04/.06$sec, because less elastic strain is available for release during unloading. Figure 34 compares load -strain curves between an element with plastic deformation and one without. The two curves do not return to zero load because P_{max} consists of both in situ and weapons effect loading. Note that the element in the plastic zone is straining 3 to 4 times more than the elastic element. Although a large portion of the plastic element's strain is recovered, some irreversible strain is present. This plastic strain is caused by slippage, crushing, and rearrangement of rock particles.

Figures 35-38 compare σ_y stresses along a 45° radial for the two load cases with varying γ. Figures 39-42 compare σ_x stresses in a similar fashion. The 1/4 kbar stresses of Figs 35 and 36 converge as distance away from the cutout increases, because only 15% of the vertical load is

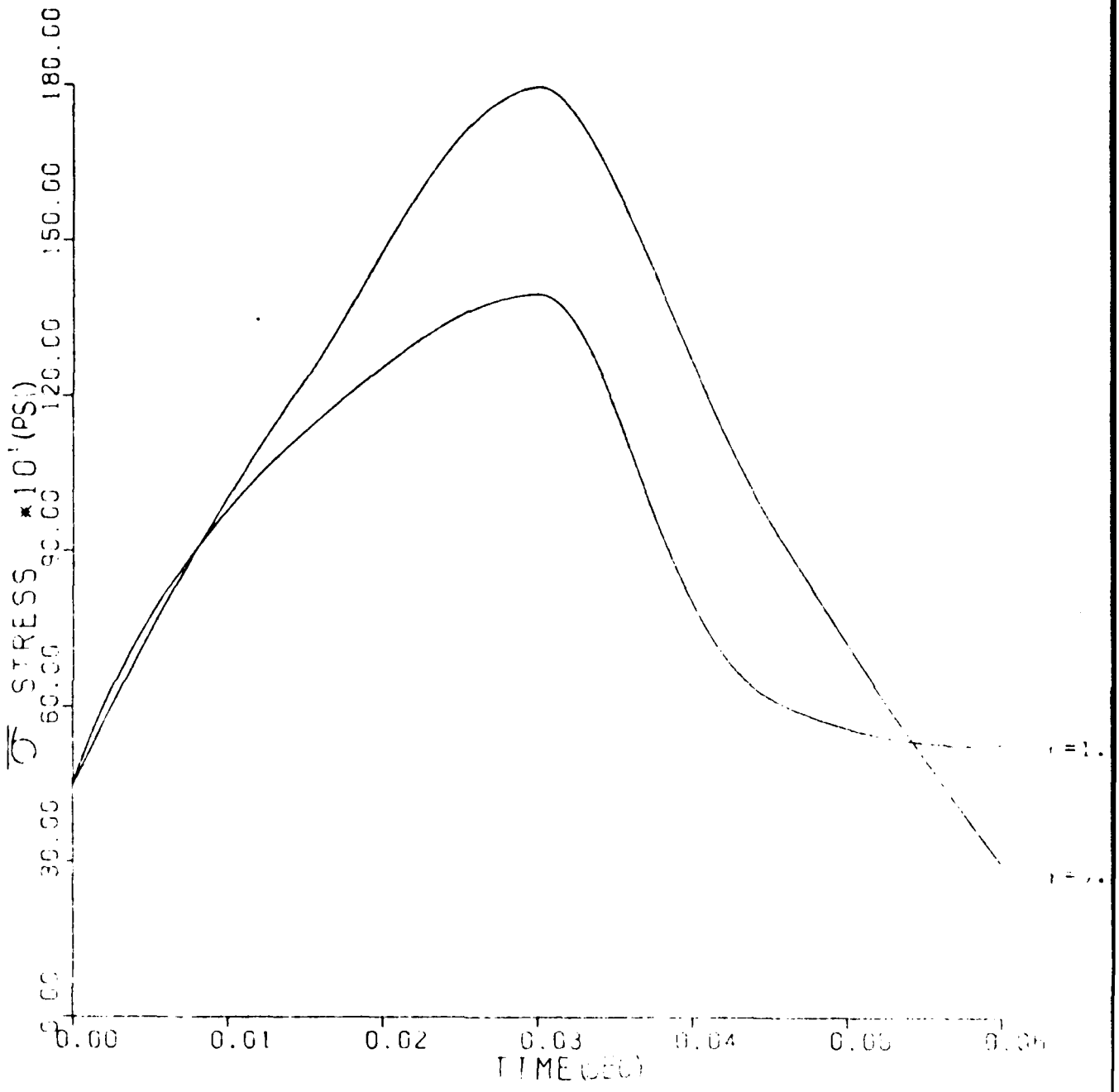

Fig 32. Effective Stress -- 1/4 kbar,
γ = 0.1, γ = 1.0

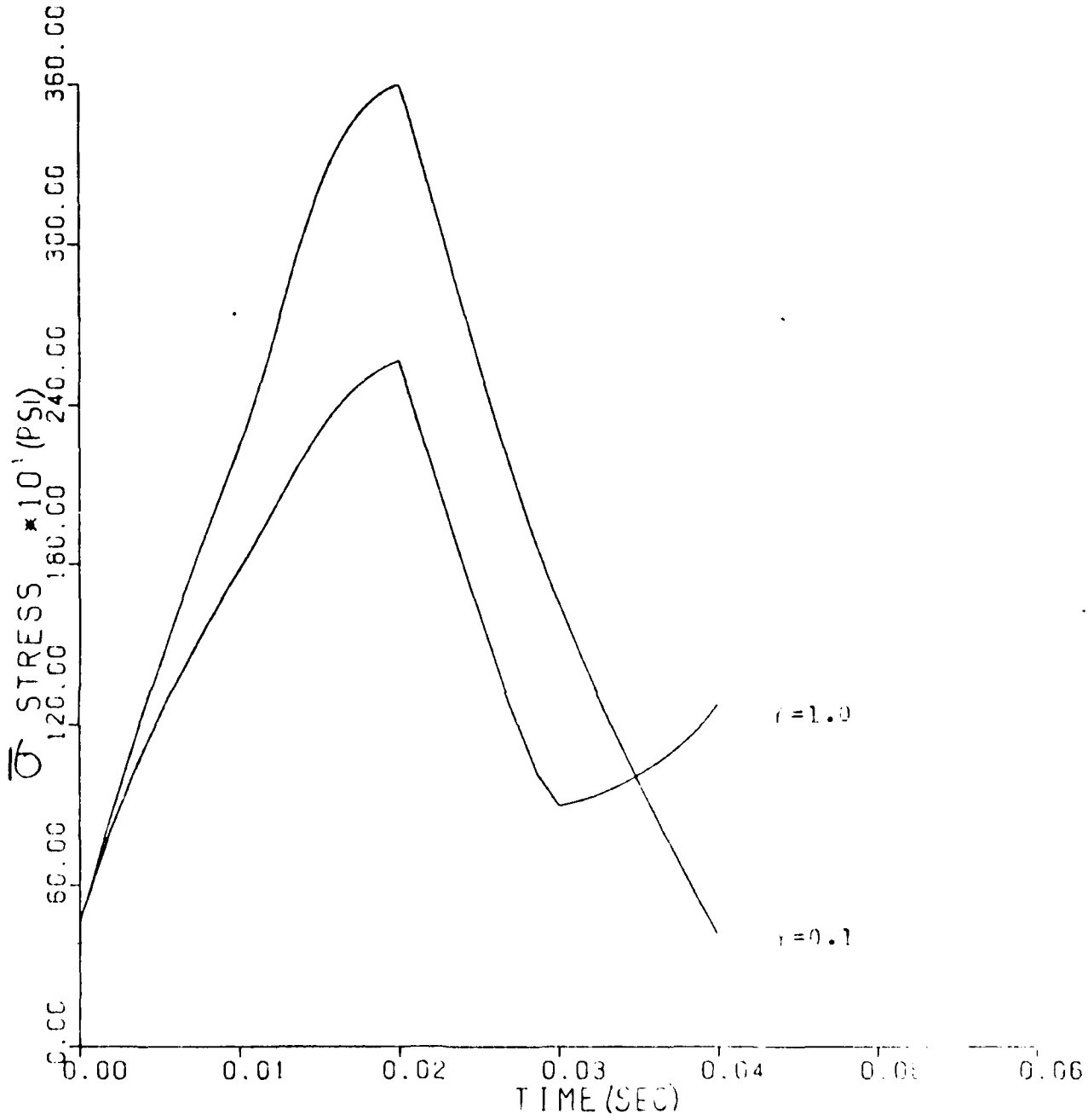

Fig 33. Effective Stress $\bar{\sigma}$ --1/2 kbar, $\gamma = 0.1$, $\gamma = 1.0$

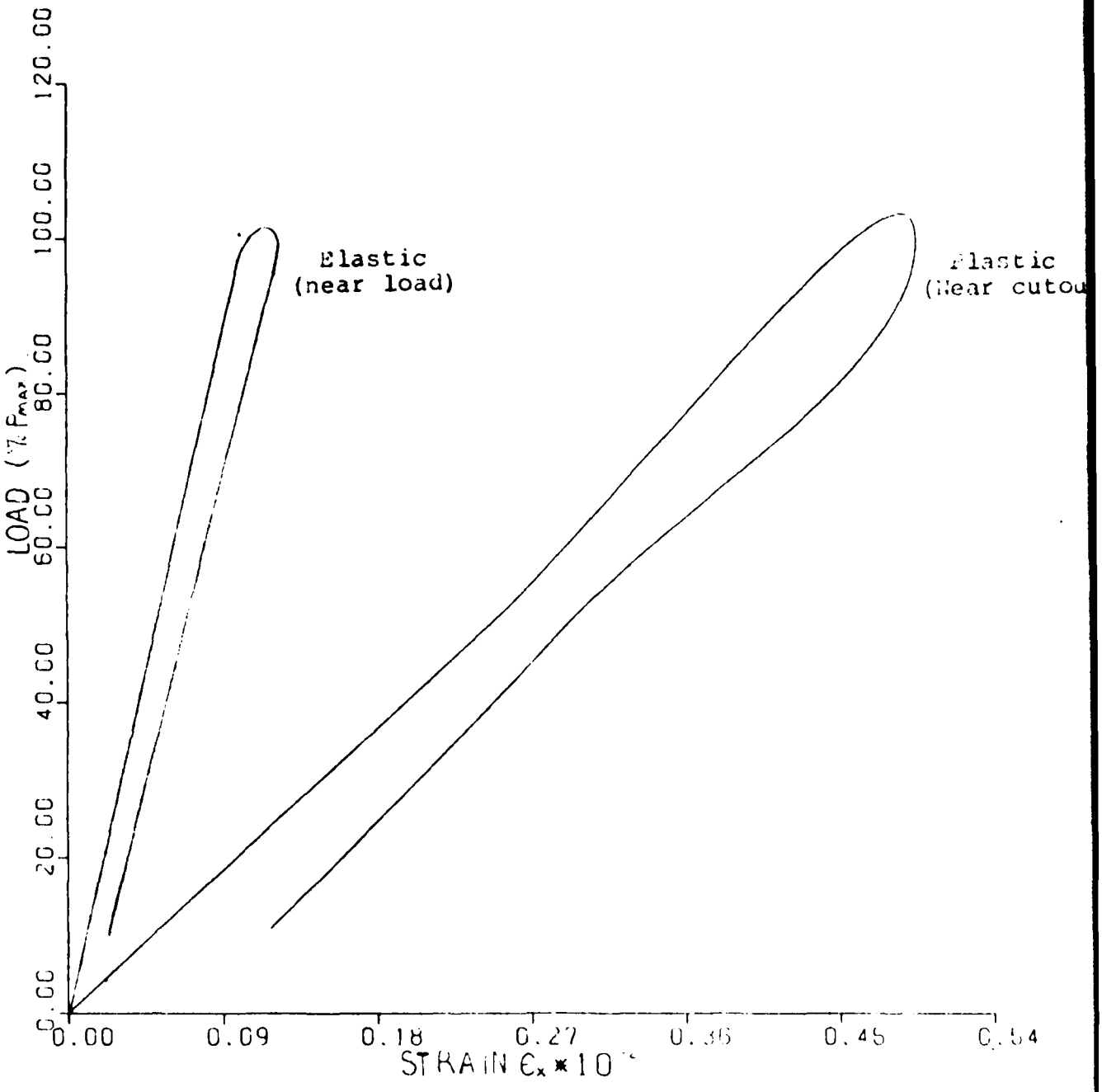

Fig 34. Plastic/Elastic Strain vs. Load Curves

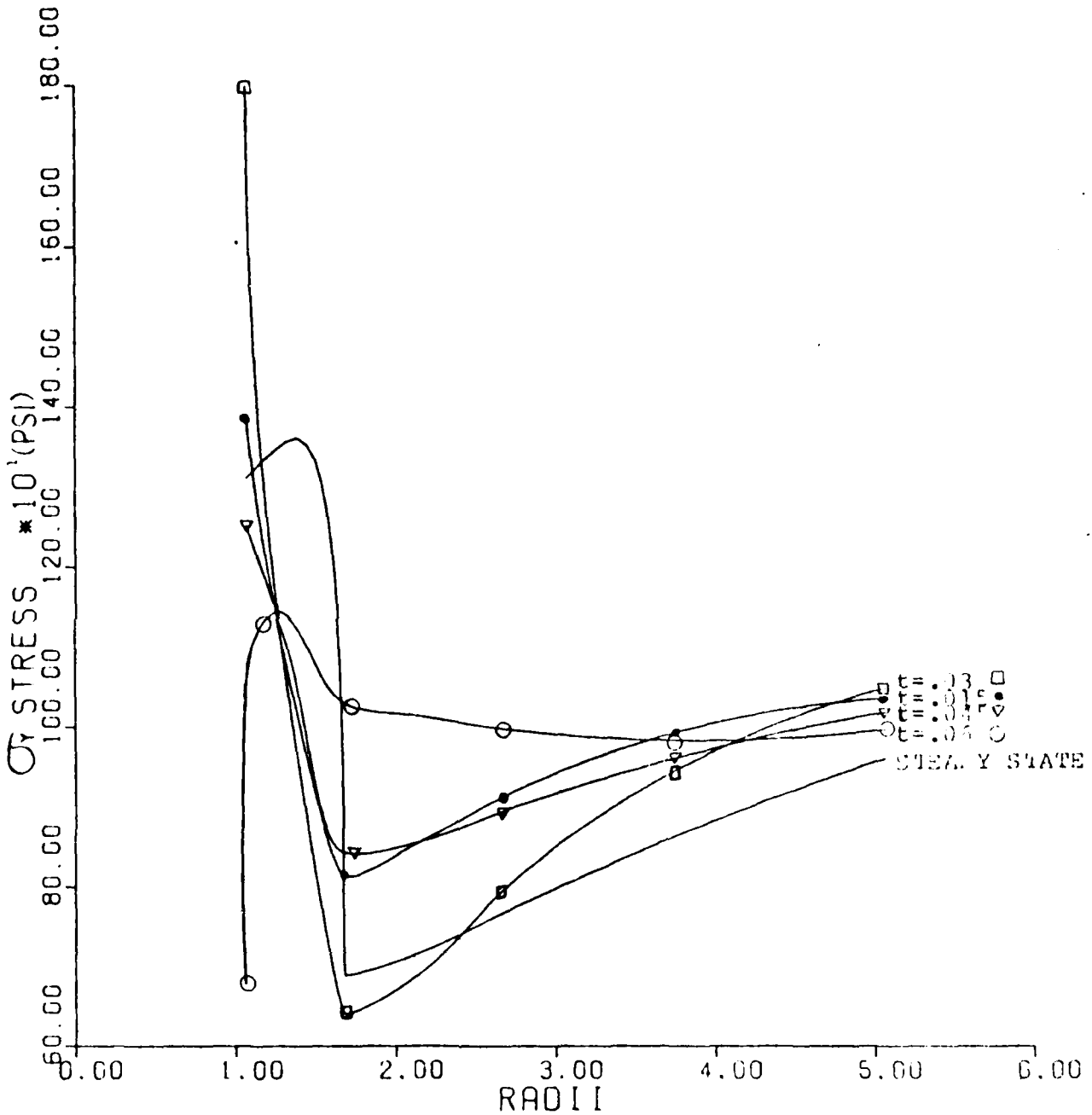

Fig 35. σ_y as a Function of Time Along 45° Radial, 1/4 kbar, $\gamma = 0.1$

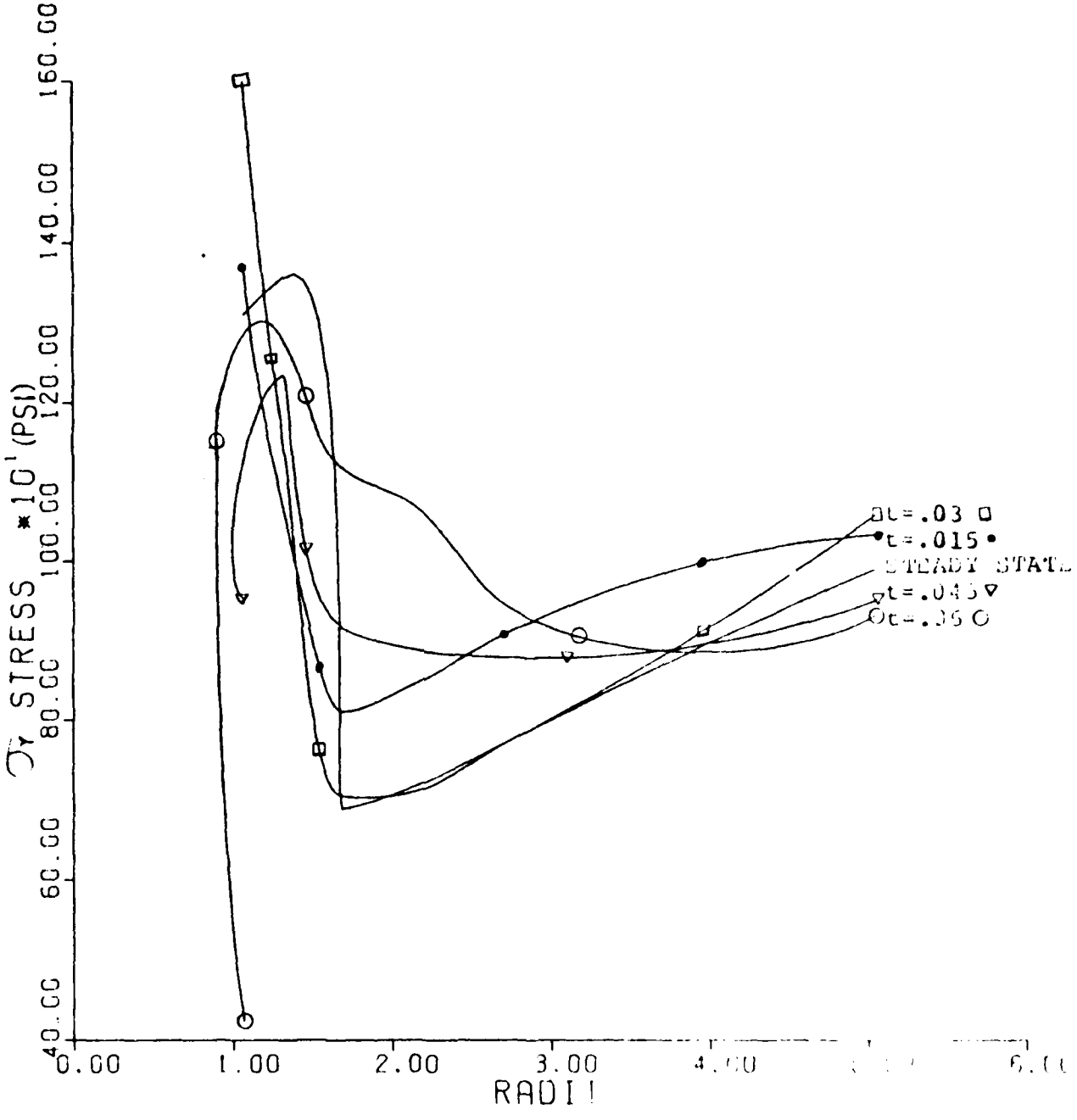

Fig 36. σ_y as a Function of Time Along 45° Radial, 1/4 kbar, γ = 1.0

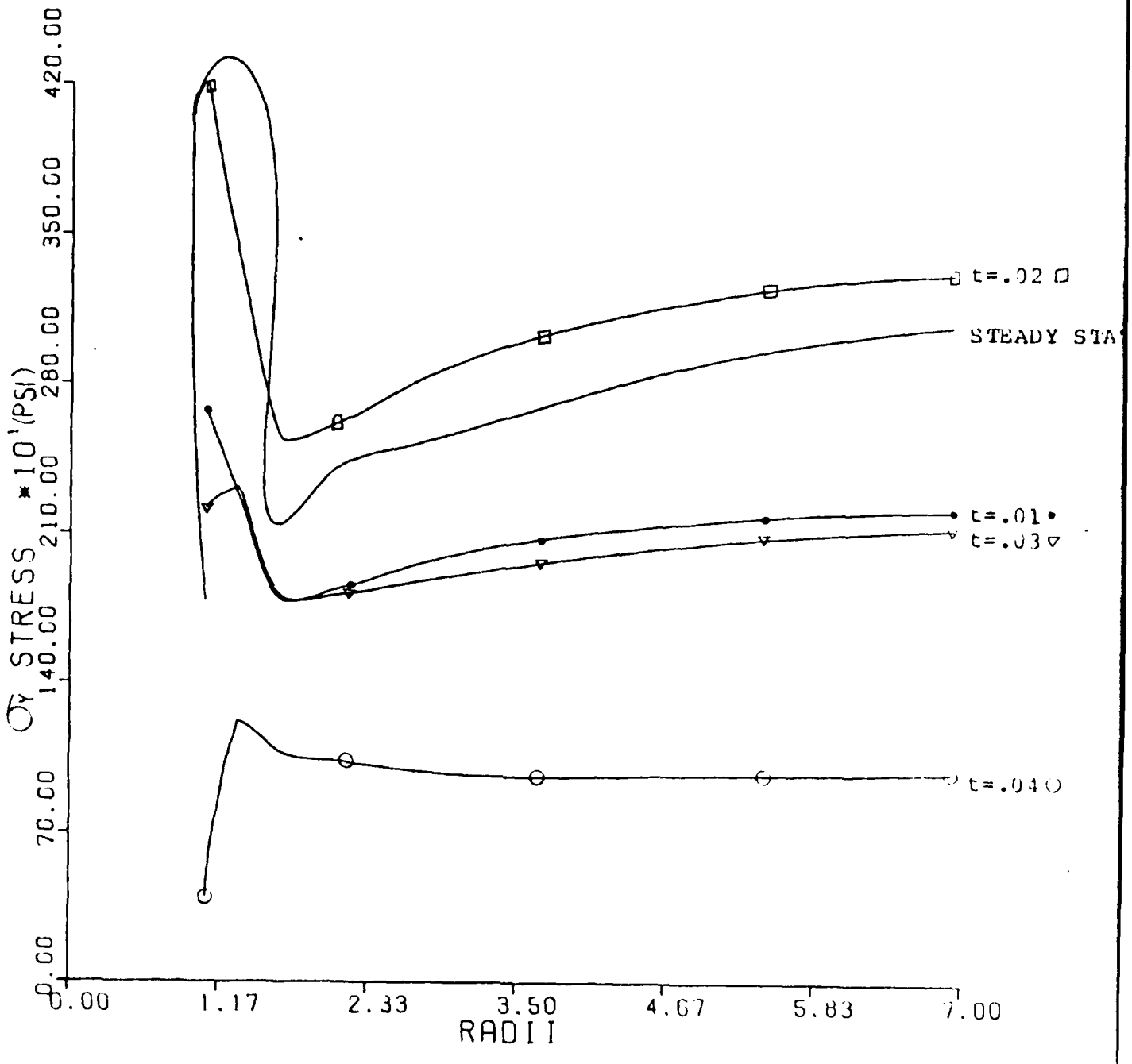

Fig 37. σ_y as a Function of Time Along 45° Radial, 1/2 kbar, $\gamma = 0.1$

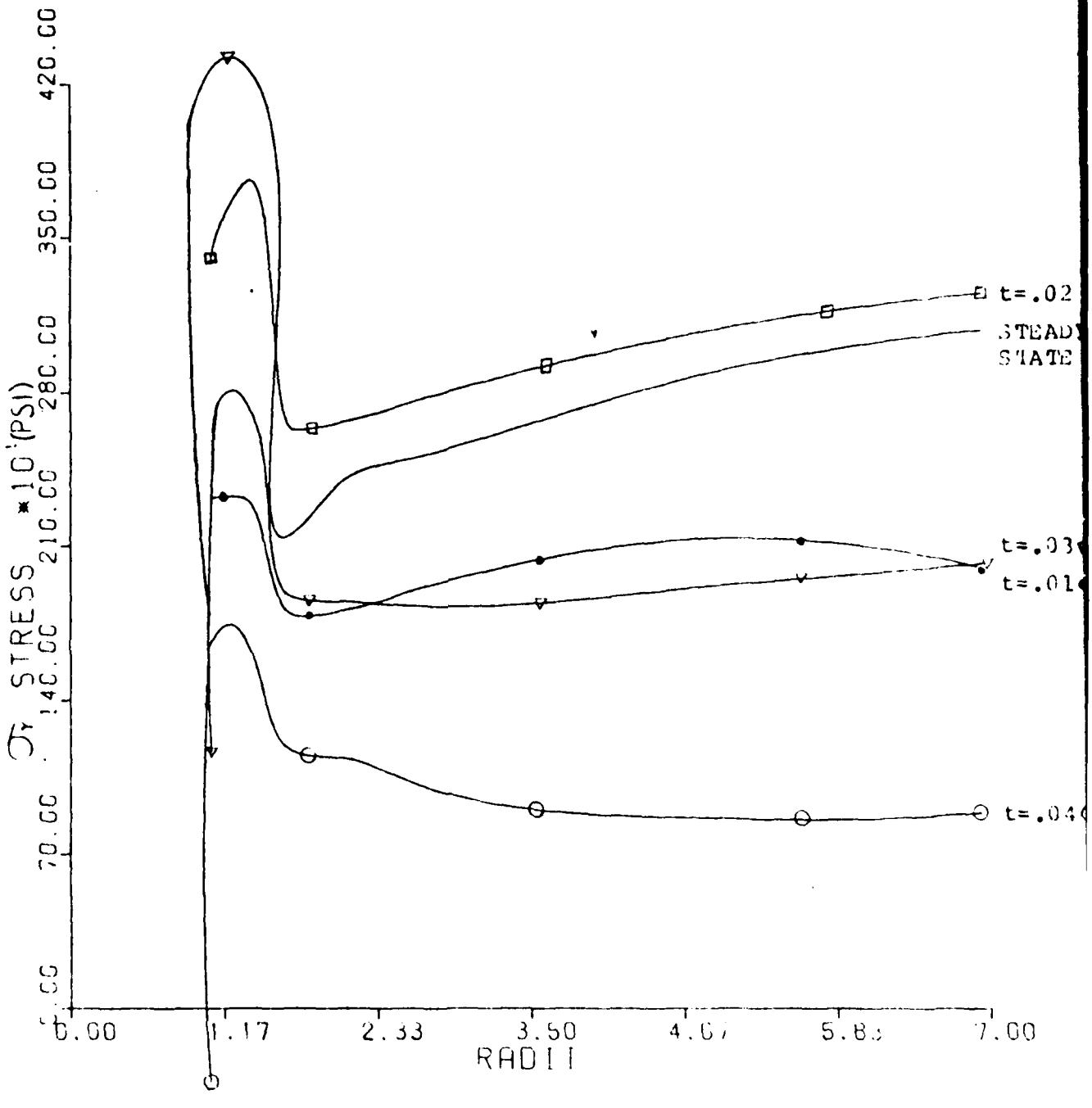

Fig 38. σ_y as a Function of Time Along 45° Radial, 1/2 kbar, , = 1.0

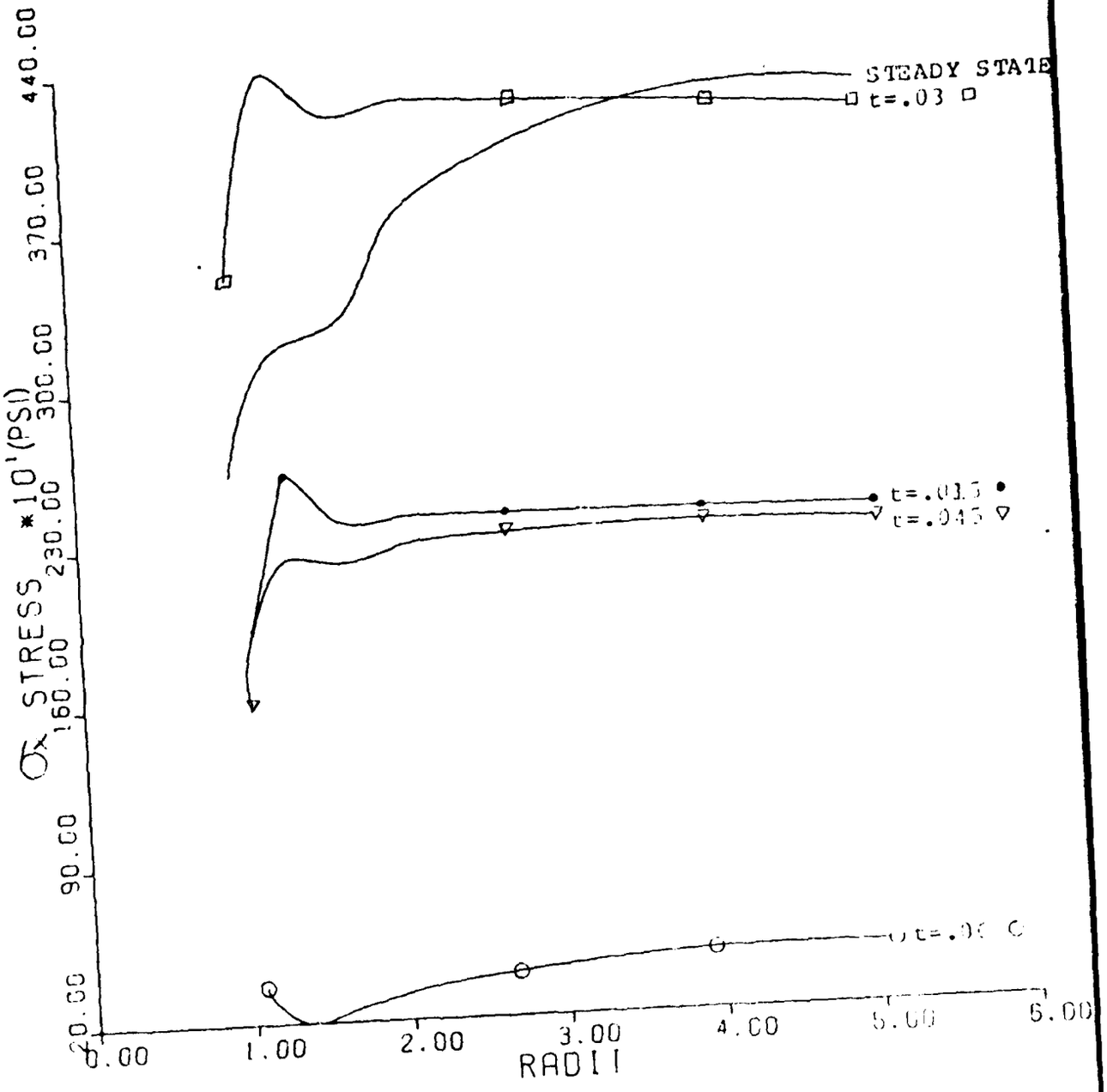

Fig 39. σ_x as a Function of Time Along 45° Radial, 1/4 kbar, $\gamma = 0.1$

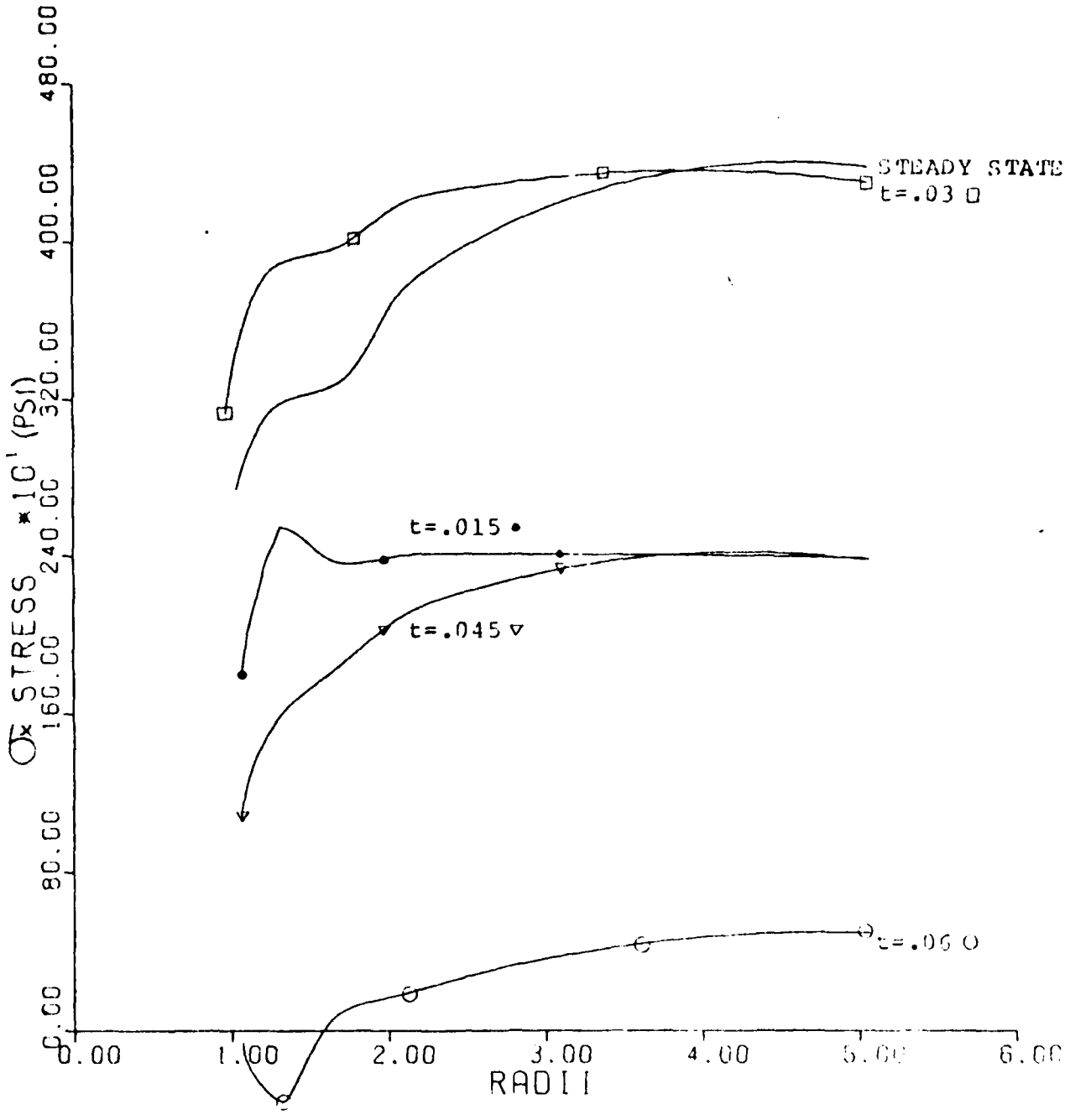

Fig 40. σ_x as a Function of Time Along 45° Radial, 1/4 kbar, $\gamma = 1.0$

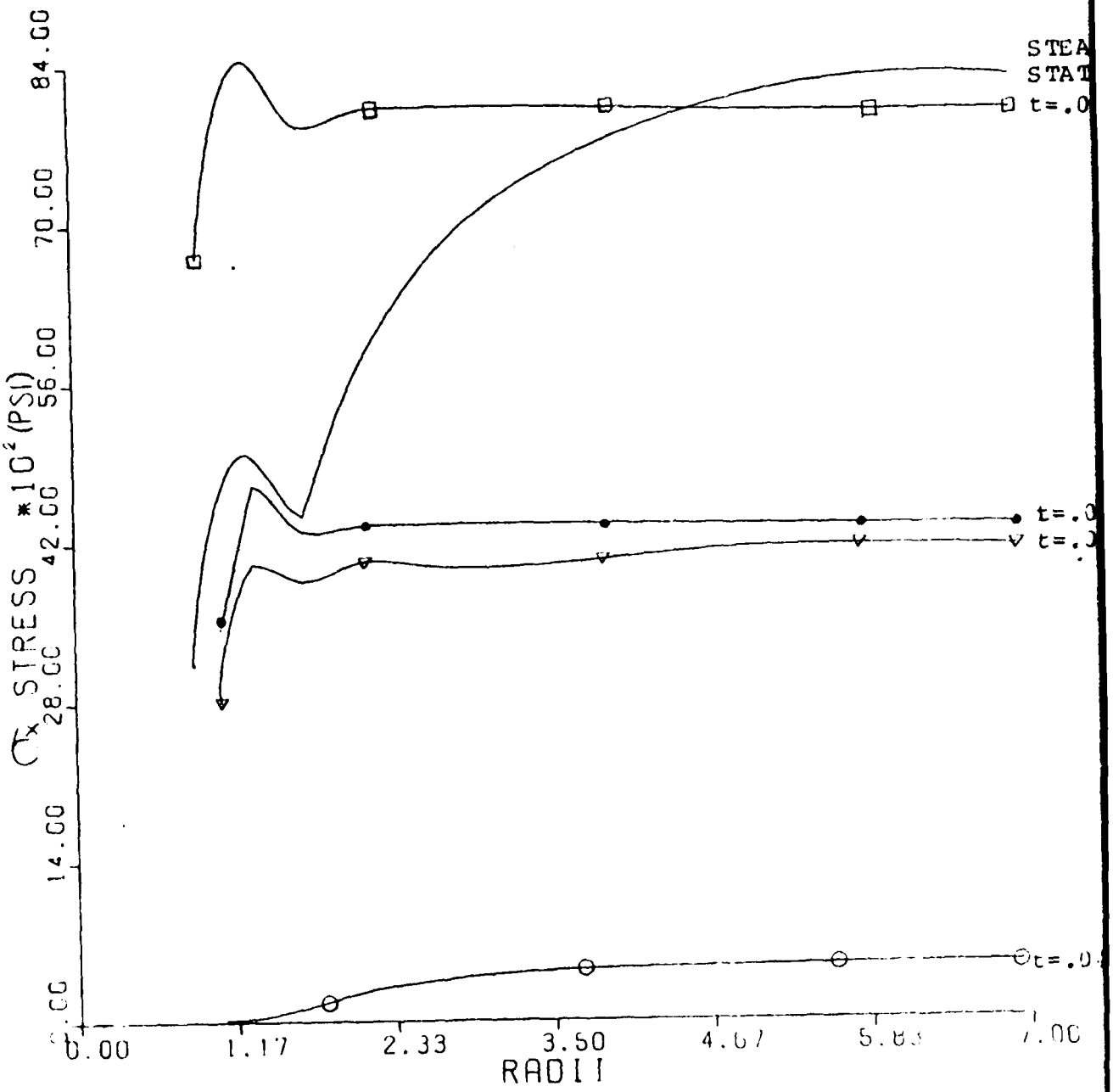

Fig 41. σ_x as a Function of Time Along 45° Radial, 1/2 kbar, $\gamma = 0.1$

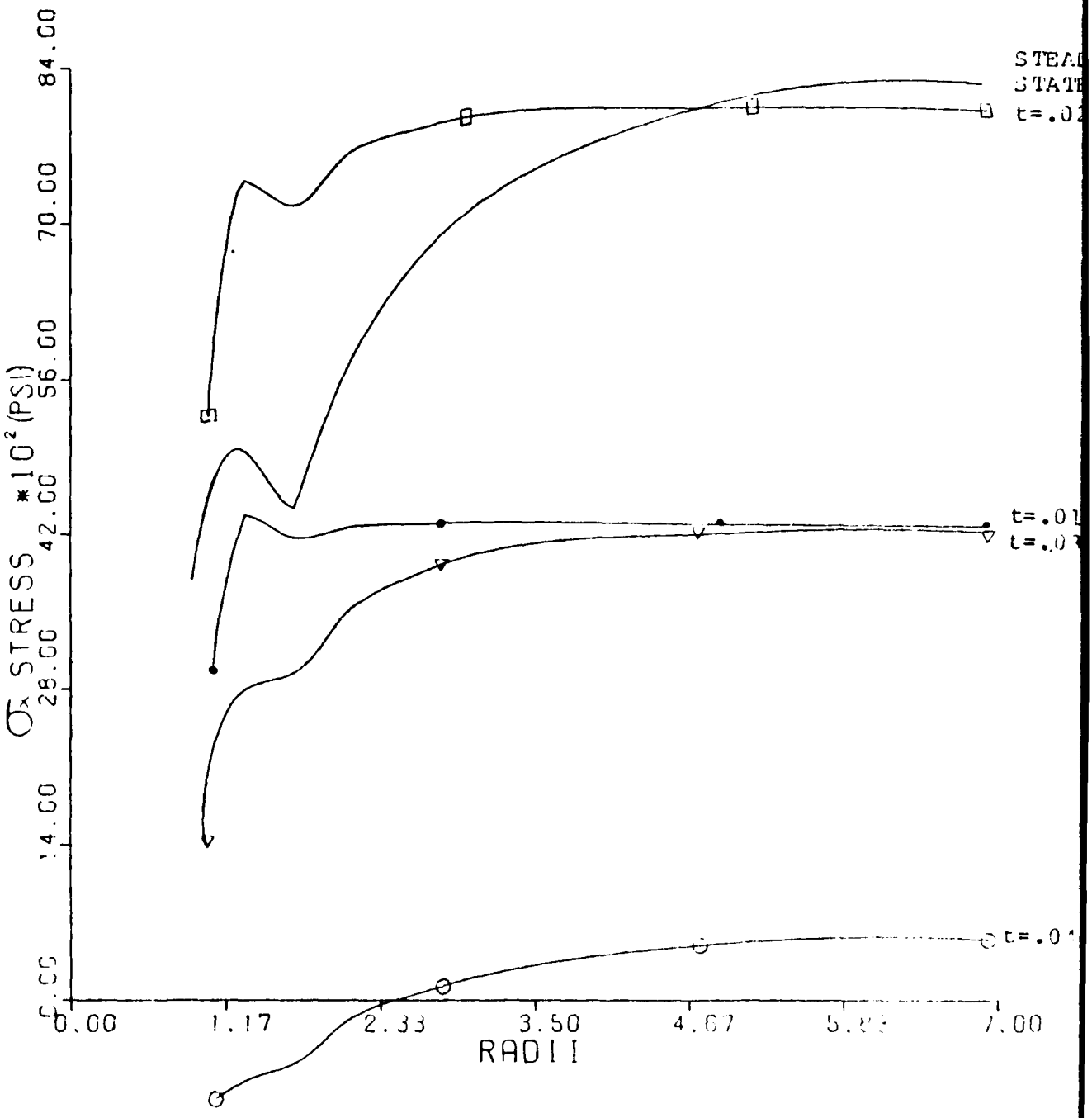

Fig 42. σ_x as a Function of Time Along 45° Radial, 1/2 kbar, $\gamma = 1.0$

varying with time. Eighty-nine percent of the 1/4 kbar horizontal load varies with time; respective percentages for 1/2 kbar loading are 72% and 95%, explaining the much greater variability in final stresses (Figs 37-42). Note in all cases that maximum stresses (at t = .03 for 1/4 kbar, and t = .02 for 1/2 kbar) near the cutout exceed the steady state stresses. One would expect the component stresses to follow $\bar{\sigma}$, i.e., stresses at t = .03 for the 1/4 kbar case (t = .02 for 1/2 kbar) should be a maximum. However, note in Figs 35 and 36 that t = .03 (1/4 kbar) stresses are not consistently the highest. This is another example of the redistribution of stresses afforded by plastic action.

Finally, note that Figs 40 and 42 show tension (negative values) for arithmetic average σ_x stresses between elements for $\gamma = 1.0$, 1/4 and 1/2 kbar loading. Although some tension was developed in the static analysis, the tension developed for the transient case is much more severe. The 1/2 kbar case, for example, developed 91 tension elements; these instantaneous tensile stresses may cause cracks which will not close due to in situ loading after the pressure wave passes, leading to zones of fallen rock in the tunnel.

A Final Note

Bishop (Ref 1) suggests that the Drucker-Prager yield criterion allows excessive plastic flow. Bishop further

intimates that this plastic strain error is due to the fact that large volumetric strains are allowed to occur. From Eq (2.14)

$$\dot{\varepsilon}_{ij}^{vp} = \gamma\left[\frac{\bar{\sigma}}{\bar{Y}} - 1\right]\left[a\right] \qquad (2.14)$$

where for direct (volumetric) strains

$$\dot{\varepsilon}_{ij}^{vp} = \gamma\left[\frac{\bar{\sigma}}{\bar{k}} - 1\right]\left[\frac{\bar{\sigma}'_{ij}}{2(J_2')^{\frac{1}{2}}} + \alpha\right] \quad (i = j) \qquad (2.15)$$

Note that $\bar{\sigma} = \alpha J_1 + (J_2')^{\frac{1}{2}}$ (yield surface).

In an effort to reduce the amount of plastic volumetric strain, the α term was removed from Eq (2.15) so that

$$\dot{\varepsilon}_{ij}^{vp} = \gamma\left[\frac{\bar{\sigma}}{\bar{k}} - 1\right]\left[\frac{\bar{\sigma}'_{ij}}{2(J_2')^{\frac{1}{2}}}\right] \quad (i = j) \qquad (3.1)$$

Note that by removing α in this fashion, it is still included in the $\bar{\sigma}$ term which triggers the plastic strain rate calculation. The Baker, et al (Ref 11) in situ loading case was analyzed using Drucker-Prager in this form and compared against the earlier analysis.

Figure 43 shows the size of the plastic zone, which was the same for both forms of the yield criterion. Table 2 compares a representative stress value (σ_y) and plastic effective strain for several elements in the plastic zone, where plastic effective strain is defined as (Ref 9)

$$\varepsilon_{EFF}^{vp} = \sqrt{\frac{2}{3}\varepsilon_{ij}^{P}\varepsilon_{ij}^{P}}$$

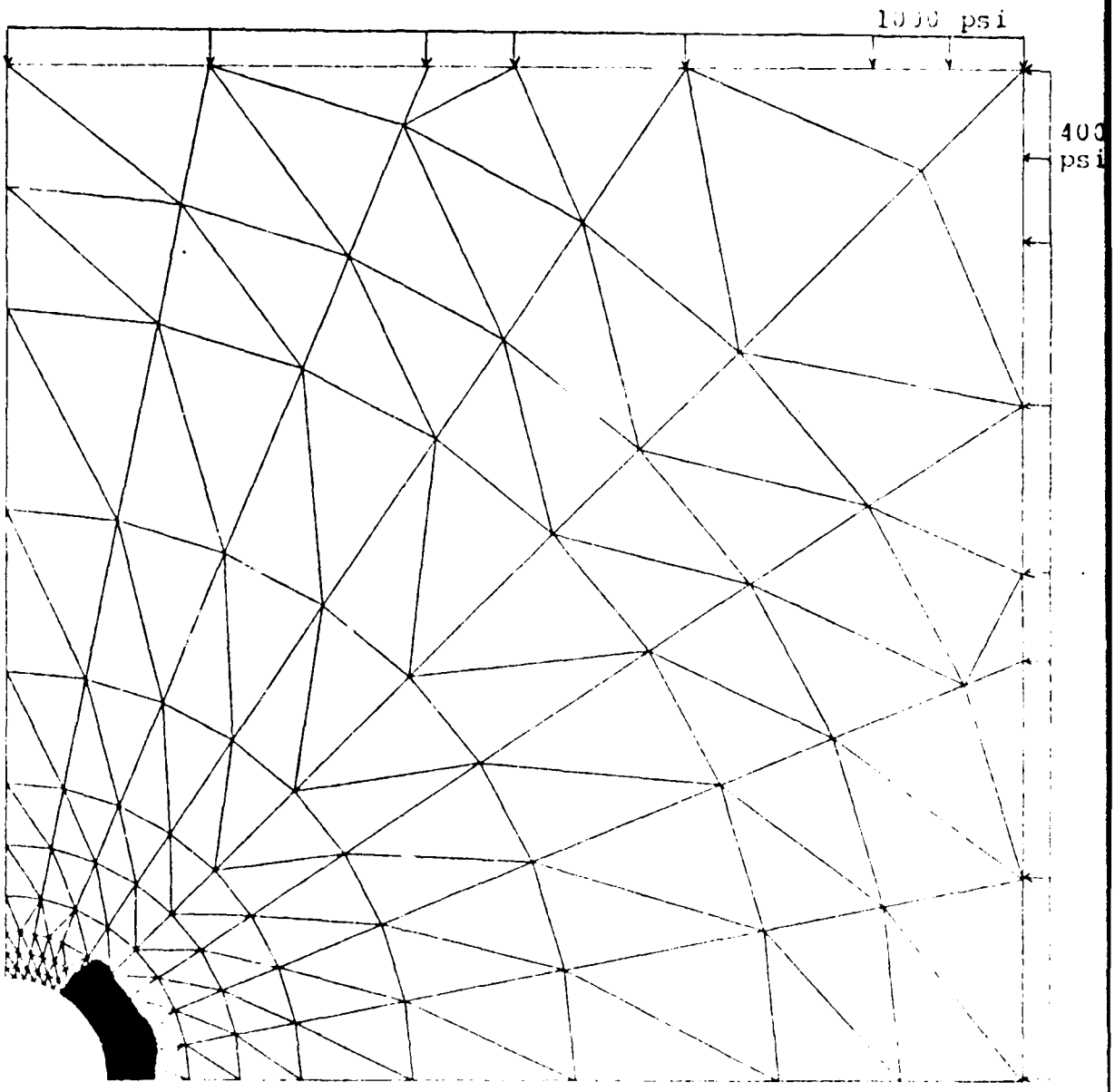

Fig 43. Plastic Zone Developed Under In Situ Load Using "Modified" Drucker-Prager Equation

Table 2 shows that the stresses (σ_x, σ_z, σ_{xy} followed a similar pattern) as well as most of the effective plastic strains were less for Eq (3.1) than for the complete Drucker-Prager equation. The validity of this form of the Drucker-Prager equations can only be proven experimentally. However, the fact that smaller effective strains are predicted is attractive.

TABLE 2

Comparing Eq (3.1) to Complete Drucker-Prager Equations

Element in Plastic Zone	Eq (3.1)		Drucker-Prager	
	σ_y	ε^{vp}_{EFF}	σ_y	ε^{vp}_{EFF}
24	1157	.00204	1328	.00367
25	813	.00183	856	.00329
26	1573	.00124	1785	.00159
27	1045	.00135	1185	.00137
28	1910	.00045	2031	.00036
29	1359	.00030	1449	.00028
30	1142	.00183	1313	.00329
31	781	.00158	833	.00290
32	1512	.00112	1705	.00134
33	974	.00083	1128	.00109

NOTE: See Fig 43 for Plastic Zone

VIII. Summary and Conclusions

A two-dimensional plane stress/plane strain finite element program called VISCO was used to model the stress field around a deep underground tunnel. The constitutive equations employed in VISCO were in the form of an elastic-perfectly plastic material model developed by Drucker and Prager. Plasticity was generated using the Drucker-Prager equations incorporated in the Malvern flow law. The following statements and conclusions are based on the analysis presented in this paper.

1. Viscoplastic theory can be used to model steady state elasto-plastic material behavior by setting the fluidity constant in the strain rate equation to a large value. Results obtained in this effort for verification purposes agreed excellently with published results.

2. It is possible to follow the effects of a nuclear blast using viscoplastic theory for both static and quasi-transient loading of tunnels buried in tuff. Results produced for the steady state conditions yielded physical activity recognized in field tests and experimental work. The transient analysis lends an appreciation of possible plastic zone growth allowing for actual experimental modification.

3. Tunnel displacements differed by extreme amounts as the load varied in the quasi-static analysis. Springline displacements were nearly eight times greater, and crown

displacements were over three times greater for 1/2 kbar versus 1/4 kbar loading. Deformations will increase as the size of the plastic zone increases.

4. In the quasi-transient analysis, the size of the plastic zone is a function of both loading and fluidity constant. The two fluidity constants used here indicate trends which may be compared against experimental results. Because the larger fluidity constant allows more plastic flow, less elastic strain is released upon unloading, creating larger final ($t = .06$, $t = .04$) tunnel displacements. For all cases (both γ and at any time) the quasi-transient model experienced less tunnel deformation than the comparable loading's static analysis.

5. Inaccurately large strains can be developed by any elastic-perfectly plastic material model. Reports show that the Drucker-Prager model may also predict excessive hydrostatic strains. A "modified" Drucker-Prager material model compared favorably against the actual equations by predicting smaller plastic strains.

Bibliography

1. Auld, Harry E. and Duane A. Labreche. "Analysis of *Tunnel Linings for Deep Basing Structures.*" AFWL-TR-80-5. Kirtland AFB, New Mexico, 1980.

2. Snitbhan, Nimitchai and Wai-Fah Chen. "Elastic-Plastic Large Deformation Analysis of Soil Slopes," Computers and Structures, 9: 567-577 (1978).

3. Bridgman, P.W. "The Effect of Hydrostatic Pressure on the Fracture of Brittle Substances," Journal of Applied Physics, 18: 246 (1947).

4. Obert, Leonard and Wilbur I. Duvall. Rock Mechanics and the Design of Structures in Rock. New York: John Wiley & Sons, Inc., 1967.

5. Owen, D.R.J. and E. Hinton. Finite Elements in Plasticity: Theory and Practice. Swansea, U.K.: Pineridge Press Limited, 1980.

6. Perzyna, Piotr. "Fundamental Problems in Viscoplasticity," Advances in Applied Mechanics. New York: Academic Press, 1966.

7. Lambe, T. William and Robert V. Whitman. Soil Mechanics. New York: John Wiley & Sons, Inc., 1969.

8. Marcal, P.V. "A Comparative Study of Numerical Methods of Elastic-Plastic Analysis," AIAA Journal, 6 (1): 157-158.

9. Hinnerichs, T.D. "Viscoplastic and Creep Crack Growth Analysis by the Finite Element Method." AFWAL-TR-80-4140. Wright-Patterson AFB, Ohio, 1981.

10. Zienkiewicz, O.C., S. Valliappan and I.P. King. "Elasto-Plastic Solutions of Engineering Problems 'Initial Stress,' Finite Element Approach," International Journal for Numerical Methods in Engineering, 1: 75-100 (1969).

11. Baker, L.E., R.S. Sandhu and W.Y. Shieh. "Application of Elasto-Plastic Analysis in Rock Mechanics by Finite Element Method," Proceedings of the 11th Symposium on Rock Mechanics. Berkeley, 1969.

12. Chen, Wai-Fah and Atef F. Saleeb. Constitutive Equations for Engineering Materials. New York: John Wiley & Sons, 1982.

13. Stagg, K.C. and O.C. Zienkiewicz. Rock Mechanics in Engineering Practice. New York: John Wiley & Sons, 1968.

14. Cook, Robert D. Concepts and Applications of Finite Element Analysis, 2d ed. New York: John Wiley & Sons, 1981.

15. Timoshenko, S. Strength of Materials, Part II, Advanced Theory and Problems, 2d ed. New York: D. Van Nostrand Company, Inc., 1947.

16. Bishop, A.W. "Strength of Soils as Engineering Materials," 6th Rankine Lecture of the British Geotechnical Society. London, 1966.

17. Means, R.E. and J.V. Parcher. Physical Properties of Soils. Columbus, Ohio: Charles E. Merrill Books, Inc., 1963.

Vita

PII Redacted

David E. Schmitz was born on [redacted] He graduated from Alameda High School in 1972 and attended the United States Air Force Academy, where he received his B.S. in Engineering Mechanics in June 1977. Shortly after commissioning, he was assigned to Kelly AFB, Texas. During his stay in Texas, he received his Masters of Business Administration from the University of Texas at San Antonio. He entered the School of Engineering, Air Force Institute of Technology in June 1981.

UNCLASSIFIED

SECURITY CLASSIFICATION OF THIS PAGE (When Data Entered)

REPORT DOCUMENTATION PAGE	READ INSTRUCTIONS BEFORE COMPLETING FORM
1. REPORT NUMBER: AFIT/GAE/AA/82D-26	2. GOVT ACCESSION NO: AD-A126640
	3. RECIPIENT'S CATALOG NUMBER
4. TITLE (and Subtitle): VISCOPLASTIC ANALYSIS OF A CONTINUOUS CYLINDRICAL OPENING SURROUNDED BY VOLCANIC TUFF	5. TYPE OF REPORT & PERIOD COVERED: MS Thesis
	6. PERFORMING ORG. REPORT NUMBER
7. AUTHOR(s): David E. Schmitz, Captain, USAF	8. CONTRACT OR GRANT NUMBER(s)
9. PERFORMING ORGANIZATION NAME AND ADDRESS: School of Engineering, Air Force Institute of Technology, WPAFB OH	10. PROGRAM ELEMENT, PROJECT, TASK AREA & WORK UNIT NUMBERS
11. CONTROLLING OFFICE NAME AND ADDRESS	12. REPORT DATE: December 1982
	13. NUMBER OF PAGES
14. MONITORING AGENCY NAME & ADDRESS (If different from Controlling Office)	15. SECURITY CLASS. (of this report): UNCLASSIFIED
	15a. DECLASSIFICATION DOWNGRADING SCHEDULE

16. DISTRIBUTION STATEMENT (of this Report)

Approved for public release; distribution unlimited

17. DISTRIBUTION STATEMENT (of the abstract entered in Block 20, if different from Report)

18. SUPPLEMENTARY NOTES

Approved for public release: IAW AFR 190-17.

LYNN E. WOLAVER
Dean for Research and Professional Development
Air Force Institute of Technology (ATC)
Wright-Patterson AFB OH 45433

14 FEB 1983

19. KEY WORDS (Continue on reverse side if necessary and identify by block number)

Viscoplasticity
Malvern Flow Law
Nuclear Blast Effects
Drucker-Prager Yield Criterion
Deep Underground Tunnel
Finite Element Modeling
Time Dependency

20. ABSTRACT (Continue on reverse side if necessary and identify by block number)

Nuclear blast effect on a deep underground tunnel was studied for quasi-static and quasi-transient loading conditions. A finite element model was developed and used with a two-dimensional constant strain triangle computer code. Viscoplasticity was introduced through the Malvern flow law in conjunction with the Drucker-Prager constitutive equations. The quasi-static results compared favorably with experimental studies. Quasi-transient results can be compared against future experimental work and field tests.

DD FORM 1 JAN 73 1473 EDITION OF 1 NOV 65 IS OBSOLETE

UNCLASSIFIED

SECURITY CLASSIFICATION OF THIS PAGE (When Data Entered)